atmosphere

MDPI

Article

Challenges and Opportunities with New Generation Geostationary Meteorological Satellite Datasets for Analyses and Initial Conditions for Forecasting Hurricane Irma (2017) Rapid Intensification Event

Russell L. Elsberry [1,*], Joel W. Feldmeier [2], Hway-Jen Chen [2,*], Melinda Peng [1], Christopher S. Velden [3] and Qing Wang [2]

[1] Trauma, Health and Hazards Center, University Colorado-Colorado Springs, Colorado Springs, CO 80918, USA; mpeng@uccs.edu
[2] Department of Meteorology, Naval Postgraduate School, Monterey, CA 93943, USA; jwfeldme1@nps.edu (J.W.F.); qwang@nps.edu (Q.W.)
[3] Cooperative Institute Meteorological Satellite Studies, Madison, WI 53706, USA; chris.velden@ssec.wisc.edu
* Correspondence: relsberr@uccs.edu (R.L.E.); hjchen@nps.edu (H.-J.C.)

Received: 15 September 2020; Accepted: 30 October 2020; Published: 6 November 2020

Abstract: This study utilizes an extremely high spatial resolution GOES-16 atmospheric motion vector (AMV) dataset processed at 15 min intervals in a modified version of our original dynamic initialization technique to analyze and forecast a rapid intensification (RI) event in Hurricane Irma (2017). The most important modifications are a more time-efficient dynamic initialization technique and adding a near-surface wind field adjustment as a low-level constraint on the distribution of deep convection relative to the translating center. With the new technique, the Coupled Ocean/Atmospheric Mesoscale Prediction System for Tropical Cyclones (COAMPS-TC) model initial wind field at 12.86 km elevation quickly adjusts to the cirrus-level GOES-16 AMVs to better detect the Irma outflow magnitude and areal extent every 15 min, and predicts direct connections to adjacent synoptic circulations much better than a dynamic initialization with only lower-resolution hourly GOES-13 AMVs and also better than a cold-start COAMPS-TC initialization with a bogus vortex. Furthermore, only with the GOES-16 AMVs does the COAMPS-TC model accurately predict the timing of an intermediate 12 h constant-intensity period between two segments of the Irma RI. By comparison, HWRF model study of the Irma case that utilized the same GOES-16 AMV dataset predicted a continuous RI without the intermediate constant-intensity period, and predicted more limited outflow areal extents without strong direct connections with adjacent synoptic circulations.

Keywords: tropical cyclone rapid intensification; geostationary meteorological satellite datasets; assimilation of atmospheric motion vectors

1. Introduction

This contribution to this special issue on data assimilation for tropical cyclone (TC) forecasts will focus on the opportunities for improved initial conditions utilizing high spatial and temporal resolution atmospheric motion vectors (AMVs) that are now derivable from the new-generation geostationary meteorological satellite GOES-16. Elsberry et al. (2018) [1] utilized a dynamic initialization technique to initialize the Coupled Ocean/Atmospheric Mesoscale Prediction System for Tropical Cyclones (COAMPS-TC) and the Naval Global Environment Model (NAVGEM) with special GOES-13 AMV datasets reprocessed by the Cooperative Institute for Meteorological Satellite Studies (CIMSS) at 15 min intervals. The focus of that Elsberry et al. [1] study was on analyses and forecasts of the

interruption of the rapid decay and subsequent constant-intensity period of Hurricane Joaquin (2015). Hendricks et al. (2018) [2] utilized a set of 15 min CIMSS Vertical Wind Shear (VWS-C) analyses based on that reprocessed AMV dataset to document the large (~15 m s^{-1}) VWS-C throughout most of the decay period of Hurricane Joaquin. Hendricks et al. [2] also demonstrated a unique dataset of the High-Definition Sounding System dropwindsondes deployed from the NASA WB-57 aircraft that the Joaquin vortex tilt structure and inner-core potential temperature anomalies in the vertical were consistent with the VWS-C variations in magnitude and direction.

Elsberry et al. (2020) [3] also utilized that 15 min VWS-C dataset during the entire lifecycle of Hurricane Joaquin to examine four intensity change events including two rapid intensifications (RIs) and two decays and four intensity change segments immediately before or after the four events. Rather than comparing with the National Hurricane Center (NHC) six-hourly intensity changes based on their best track, Elsberry et al. [3] found higher correlations of the VWS-C dataset with the 30 min interval CIMSS Satellite Consensus (SATCON) intensity changes.

The first Joaquin RI, which had a peak intensity change of 16 kt/6 h according to the SATCON, was shown to occur after only a small (2 m s^{-1}) decrease in the VWS-C into the moderate range that Elsberry et al. [3] defined as 8 m s^{-1}. Following that first RI event, the RI continued at a smaller rate for approximately 30 h, at which time Joaquin reached its first peak intensity of 120 kt [4]. The correlation coefficient between these continued positive intensity increases and the VWS-C magnitude was negative, and Elsberry et al. [3] documented that there was also a rotation of the VWS-C direction to become more aligned with the southwestward heading of Joaquin. During the track reversal of Joaquin (see Figure 1 in Elsberry et al. [3]), the intensity of Joaquin decreased when the VWS-C was also decreasing (positive correlation rather than the expected negative correlation), which Elsberry et al. [3] explained was consistent with the ocean cooling induced within the anticyclonic track loop during the prior southwestward track. The second Joaquin RI, which began as Joaquin moved poleward beyond the ocean-cooled region, was as a mature hurricane with an intensity of 110 kt increasing to an intensity of 135 kt [4]. Rather than this positive intensity change being associated with a negative VWS-C deviation, the peak intensity increase of 15 kt/6 h slightly leads in time a rapid VWS-C increase (positive correlation) as Joaquin is translating northeastward toward an adjacent upper-tropospheric cyclone. Elsberry et al. [3] conclude that the alternating negative and positive correlations between the high temporal resolution (15 min) VWS-C and (30 min) SATCON intensity changes demonstrate short-term nonlinear relationships that must be analyzed and modeled to improve TC intensity forecasts, and especially RI event timings and magnitudes.

The CIMSS has reprocessed another special high temporal resolution (15 min interval) AMV dataset only now from the GOES-16 Advanced Baseline Imager (ABI) for Hurricane Irma (2017) [5]. In addition to the routine GOES-16 full-disk scan every 10 min and the Continental U.S. scanning every 5 min, the TC-following mesoscale scan mode allows one-minute scanning and was focused on Irma's center with a 10° latitude by 10° longitude domain [6,7]. Using this one-minute imagery, CIMSS has developed automated algorithms to produce enhanced (very high spatial resolution) AMVs. The CIMSS special processing strategies allowed by the 1 min image scanning greatly enhance the AMV coverage to resolve the small scales of the flow fields associated with the Irma vortex and its near environment. An example is shown in Figure 1, which depicts specially-processed GOES-16 meso scan AMVs (Figure 1b) in comparison to the routinely-processed AMVs derived from GOES-13 (Figure 1a).

In their contribution to this special issue on data assimilation for tropical cyclone forecasts, Lewis et al. (2020) [6] explore different strategies for assimilation of this special GOES-16 AMV dataset to improve the Hurricane Weather Research Forecast (HWRF) track, intensity, and structure (i.e., wind radii) forecasts. The CIMSS has kindly provided this special GOES-16 AMV dataset to our research group to examine the Irma RI event with the dynamic initialization scheme used for the Elsberry et al. [1] study of Hurricane Joaquin. The focus of this study with these GOES-16 AMVs is an Irma RI that began on 4 September and continued to midday on 5 September, by which time Irma had strengthened from 100 kt to a category-5 hurricane with maximum sustained winds of 155 kt [5].

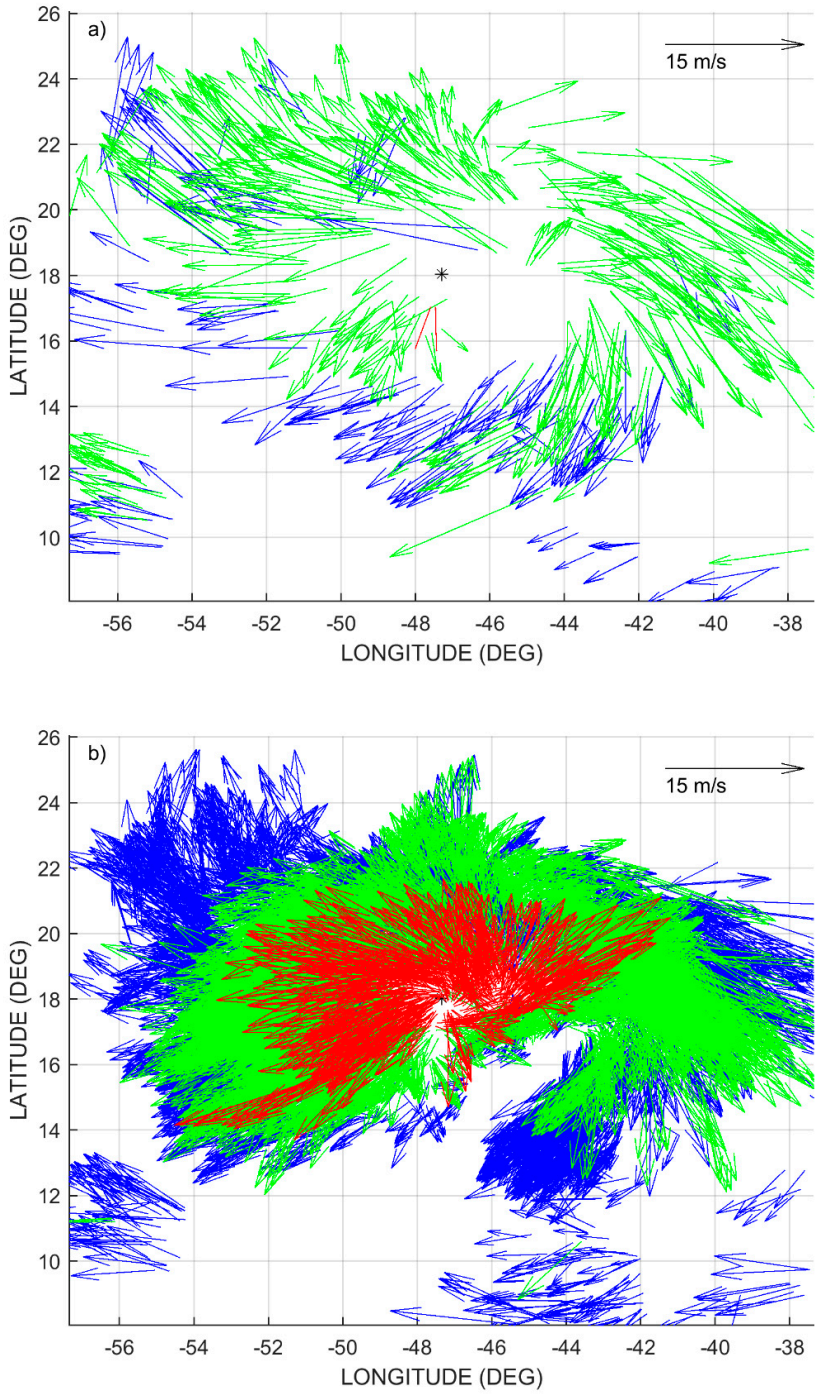

Figure 1. (**a**) Internal CIMSS hourly AMVs from GOES-13 at 0900 UTC 3 September relative to the Hurricane Irma position (asterisk) with green (blue) vectors between 150 and 200 mb (200 and 250 mb). (**b**) As in panel (**a**), except for CIMSS 15 min AMVs from GOES-16 at 0915 UTC 3 September with addition of AMVs above 150 mb in red vectors.

Exciting opportunities now exist to observe, monitor, and analyze the Irma RI event with the high spatial resolution GOES-16 AMVs. The lower-resolution hourly AMVs from the GOES-13 do detect multiple outflow regions in the 150–200 mb layer (Figure 1, green vectors) and the 200–250 mb layer (blue vectors), but with the exception of several small wind vectors near the center, only at large distances from the center. The specially-processed GOES-16AMVs using the one-minute imagery within the meso scan domain [7] resolve these outer AMVs at much higher spatial resolution. More importantly,

these AMVs can depict the inner-core outflow at elevations above 150 mb (red vectors) and help define the "outflow dome" that is highly asymmetric.

The assimilation challenges are to ingest these extremely high spatial density AMVs each 15 min and retain their information to capture the Irma vortex structure and intensity changes. A number of these challenges that had to be addressed to assimilate the GOES-16 AMVs in the Elsberry et al. [1] technique will be described in Section 2. The focus in this study will be on the first six-hour data assimilation period during which the GOES-16 AMVs were available from the meso scans. The benefits of assimilating these 15 min AMV datasets versus incorporating only the hourly GOES-13 AMV datasets as in Figure 1a will be presented in Section 2. The subsequent 72 h COAMPS-TC forecasts from the hourly AMV-based initial conditions versus the 15 min GOES-16 AMVs initial conditions will also be presented to illustrate the improved predictions of the Irma RI. The CIMSS has also provided the HWRF initial conditions at the end of the same six-hour data assimilation period with full meso scan domain GOES-16 AMVs, and the subsequent 72 h HWRF forecast as described in Lewis et al. [6]. These HWRF initial conditions and the HWRF forecast during the Irma RI will be compared in Section 3 with the modified Elsberry et al. [1] dynamic initialization approach in Section 2. A summary and concluding remarks will be given in Section 4.

2. Data Assimilation Techniques for High-Density AMVs

2.1. Modifications to the Elsberry et al. Dynamic Initialization

2.1.1. New FCDI Dynamic Initialization Technique

The key component in the Elsberry et al. [1] dynamic initialization was the Spline Analysis at Mesoscale Utilizing Radar and Aircraft Instrumentation (SAMURAI; Bell et al. 2012 [8]), which had been adapted to first spread the AMV speed and direction information horizontally and vertically to the COAMPS-TC grid points. The SAMURAI is a three-dimensional variational analysis that minimizes an incremental form of a cost function using a finite-element approach with cubic spline elements as a basis. The SAMURAI has three spatial filters that act as a background error covariance to spread information from the AMV observations throughout the domain, which in Elsberry et al. [1] was the AMV-based zonal and meridional wind increments every 15 min relative to a background COAMPS-TC forecast wind field. Hendricks et al. [2] documented the AMV-based SAMURAI analysis created Joaquin vortex vertical structure and vortex tilts that were confirmed with the High-Definition Sounding System dropwindsondes. However, the SAMURAI analysis is very time consuming even with AMV densities similar to the distribution in Figure 1a, and thus a modification was necessary to assimilate the high-density AMVs as in Figure 1b.

The first modification of the Elsberry et al. [1] approach has been to adopt the Four-Dimensional Data Assimilation (FDDA) technique [9], which has been found to be a more straight-forward and efficient technique for assimilating the high temporal and spatial resolution AMVs in the COAMPS-TC dynamic initialization technique. In the FDDA approach, the wind fields are nudged to the AMVs by adding a nudging term to the velocity equations:

$$\frac{\partial \boldsymbol{V}(x)}{\partial t} = other\ effects + \alpha \boldsymbol{V}_{inc}(x), \tag{1}$$

where $\frac{\partial V(x)}{\partial t} = other\ effects$ represents the combination of the original prognostic equations of u and v in the COAMPS-TC, $\boldsymbol{V}(x)$ is the model velocity at grid point x, α is the nudging coefficient, and $\boldsymbol{V}_{inc}(x)$ is the increment at the model grid point x calculated as:

$$\boldsymbol{V}_{inc}(x) = \sum_{i=1}^{N} W_i^2\,(x)(\boldsymbol{V}_{AMV} - \boldsymbol{V}_C)_i / \sum_{i=1}^{N} W_i\,(x)\,, \tag{2}$$

where N is the number of AMVs, $\boldsymbol{V}_{AMV}$ is the AMV; $\boldsymbol{V}_C$ is the COAMPTS-TC model velocity interpolated to the AMV position, and $W_i(x)$ is the weighting function of the ith AMV at grid point x. The $W_i(x)$ can be obtained by multiplying the horizontal weighting (w_h) with the vertical weighting (w_v), i.e., $W_i(x) = w_h \times w_v$, where

$$w_h = \begin{cases} \frac{R^2-D^2}{R^2+D^2}, & D \le R \\ 0, & D > R \end{cases}, \quad (3)$$

and

$$w_V = \begin{cases} 1, & \text{adjacent model levels} \\ 0, & \text{levels other than adjacent levels} \end{cases} \quad (4)$$

R is the radius of influence and D is the distance from the AMV observation to the COAMPS-TC grid point.

With the high spatial density of the AMVs in the inner-core region of Irma in Figure 1b, the radius of influence R is set to be 50 km. Depending on the magnitude of R, the effective number (N_e), which is the number of AMVs with $D \le R$, of AMVs at the outflow level, or at low levels beyond the TC cirrus canopy, may be more than 100, but under the cirrus canopy and in the mid-troposphere where no AMVs are available, N_e will be equal to zero.

In principle, the AMV increment should be given a large vertical weighting value w_v at the corresponding pressure level in the COAMPS-TC model. Although the AMVs are reported to the nearest 1 mb, they are considered to represent the wind averaged over some layer thickness. Thus, the $\boldsymbol{V}_C$ has been interpolated in the vertical between the two adjacent vertical pressure levels at the horizontal grid point, and then that wind increment $(\boldsymbol{V}_{AMV} - \boldsymbol{V}_C)$ has been assigned to both adjacent levels with a w_v = 1.0. Note that Elsberry et al. [1] found that the SAMURAI wind increments were of magnitude of 1–6 m s^{-1}, and that the horizontal weighting factor (Equation (3)) will have a much larger influence than the vertical weighting factor (Equation (4)).

In summary, rather than a call to a separate SAMURAI subroutine to calculate the three-dimensional field of AMV-based wind increments to nudge the COAMPS-TC wind forecast as in Elsberry et al. [1], the raw AMVs are inserted into the COAMPS-TC model with direct calculation of the nudging term in Equation (1). That 3D field of AMV-based nudging effects will be fixed during the COAMPS-TC dynamic initialization until the next set of AMVs becomes available, and then a new 3D field of AMV-based increments will be calculated. This fully interactive FDDA approach in the COAMPS-TC dynamic initialization will be labeled as the FCDI technique.

2.1.2. Expansion of Domain 2 and 3 for the FCDI

In Elsberry et al. [1], the triple domain grid spacing was 45 km × 15 km × 5 km. The sizes of the moveable Domains 2 and 3 in the SAMURAI analysis were kept the same size as in the COAMPS-TC forecast model, and thus were relatively small (e.g., Domain 2 was approximately 16° latitude by 16° longitude). With the new 10° latitude by 10° longitude region with high-density AMVs in lower panel of Figure 1, the second modification of the Elsberry et al. [1] dynamic initialization has been to expand the sizes of Domains 2 and 3 (Figure 2). The fixed outer Domain 1 has 361 grid points east-west and 191 grid points north-south with a grid spacing of 36 km. Domain 2 (Domain 3) has 367 (556) grid points east-west and 331 (556) grid points north-south with a grid spacing of 12 km (4 km). The HWRF initialization in Lewis et al. [6] has much smaller grid spacing with north-south spacing of Domain 1 (Domain 2/Domain 3) at 0.099° (0.033°/0.011°). In the HWRF initialization comparisons with the FCDI in Section 3, the HWRF Domain 2 (~3.3 km) fields will be compared with the FCDI Domain 3 (4 km) fields. Whereas the number of vertical layers in Lewis et al. [6] is 75, only 40 vertical layers are utilized in this study, which is likely too small and a future study will test the impact of adding multiple layers at the elevation of the Irma outflow jet.

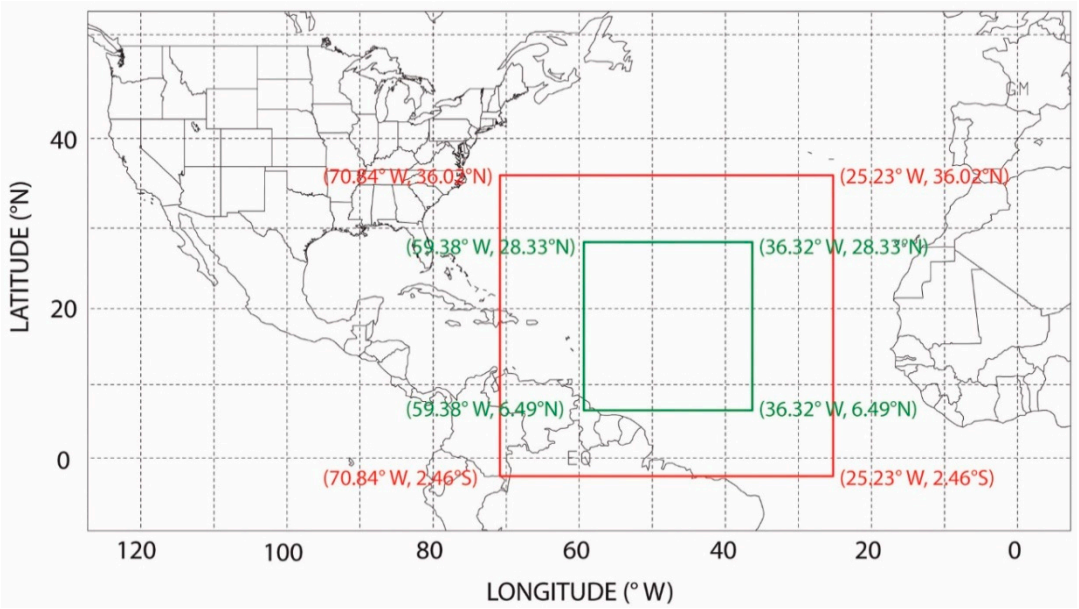

Figure 2. Three domains of the FCDI analysis of Hurricane Irma (2017) at 1200 UTC 3 September. The outer Domain 1 is fixed with 36 km grid spacing, while Domain 2 (red lines) with 12 km grid spacing and Domain 3 (green lines) with 4 km grid spacing move with the storm.

The same model physical linkages of Elsberry et al. [1] connecting intensity changes to the improved AMV depiction of the outflow are applied here to the Irma RI. First, where the AMVs are outward directed as in Figure 1 relative to the eyewall, convective cloud bands, and the cirrus cloud edges, the AMV distribution is expected to indicate divergence associated with ascent in deep convection and then the adjacent subsidence-induced clearing. In response, the model physics will infer the vertical ascent/descent and thus the convective heating distribution in the vertical and in the horizontal, which will lead to modification of the pressure (mass) field. Model dynamics will then adjust the azimuthal mean and asymmetric wind fields, which in the lower model levels will take into account the planetary boundary layer frictional effects and enthalpy fluxes. Whereas these internal adjustments will determine the intensity change (either the minimum sea-level pressure (MSLP) or the maximum near-surface wind speed (V_{max})), these TC vortex dynamics and physics predictions are also expected to improve the interaction between the vortex and its environment in conjunction with the better depiction of the outflow jets from the high temporal and spatial resolution AMVs.

A crucial aspect of the FCDI for assimilating these high temporal and spatial resolution AMVs is the two-way interaction on the three domains of the COAMPS-TC model that is forecasting the wind increments in Equation (1) of the FCDI. Elsberry et al. ([1], Figure 3) provide a schematic of the time steps on the three domains of the COAMPS-TC with two-way interaction. The time stepping begins on the 36 km Domain 1 with the appropriate FCDI wind increments. Then three time steps are taken on the 12 km Domain 2 with the FCDI wind increments on that grid. For each of these three Domain 2 time steps, three time steps are taken on the 4 km Domain 3 centered on the TC forecast position. In the two-way interaction, there are then upscale transfers of the solutions from Domain 3 to Domain 2 coincident points, and from Domain 2 to coincident points within Domain 1. During each time step on each domain, the mass (pressure) fields will be adjusted to the FCDI wind increment forcing derived for that 15 min AMV dataset. Since the time steps for Domains 1, 2, and 3 are approximately 75, 25, and 8.33 s, the FCDI with 15 min AMV datasets will have approximately 12, 36, and 108 time steps, respectively, during which the mass fields on these three domains will be adjusted to the AMV-based FCDI increments during that 15 min period. As will be demonstrated below, the largest wind increments occur in a cold start with a bogus vortex that may have wind

increments of 5–6 m s^{-1}, but depending on the nudging coefficient in Equation (1) the model winds will quickly adjust to the AMVs.

The nonlinear relationship between the Joaquin intensity changes and the AMV-based VWS-C documented by Elsberry et al. [3] provide support for the above hypothesized physical linkages. Furthermore, the Joaquin vortex tilts in association with the AMV-based VWS-C were documented by Hendricks et al. [2]. The Hendricks et al. [2] study of the decay stage, and almost all of the events in the Elsberry et al. [3] study, were when a well-established vortex in the vertical already existed under the high temporal resolution reprocessed GOES-13 AMVs. However, that pre-existing, vertically coupled vortex structure did not exist during the Joaquin first pre-RI segment [3], and thus the above hypothesized physical linkages between the cloud-top AMVs and the low-level vortex structure and boundary layer frictional effects and enthalpy fluxes were not yet well established.

2.1.3. Addition of Surface Wind Adjustment

The third modification of the Elsberry et al. [1] dynamic initialization technique was to add a surface wind field adjustment on which a 300 km by 300 km and a 1500 m deep layer centered on the TC position is used as a constraint in the regions of deep convection relative to the center, which then facilitates a connection between the boundary layer ascent with the cloud-top divergence inferred from the AMVs. In a preliminary test with Hurricane Joaquin, this "dual-constraint" connection on the deep convection horizontal and vertical distribution was particularly important for the early stages when the reprocessed GOES-13 AMVs were not sufficiently dense so as to represent well the deep convection in the rainbands (not shown). The modified Elsberry et al. [1] approach is similar to the Shewchuk and Elsberry (1978) [10] technique that adjusted the initial wind fields of an early dynamical TC model to improve the track forecast. In this Irma data assimilation application, the surface wind adjustment domain is translated every 15 min along a target pathway when a new AMV dataset becomes available. For a normal six-hour assimilation cycle, it is assumed that an accurate 6 h fix is available from the warning center, so the target pathway is simply a straight line from the t = 0 h of the assimilation cycle to that 6 h fix.

The objective of the continued adjustment of the surface wind field to move along the target pathway toward the known 6 h ending position is that the analyzed 6 h position (and the 3D vortex structure) is then sufficiently close to the next warning position that the next assimilation cycle target position may then begin from the previous assimilation 6 h position. That is, no vortex relocation or introduction of a bogus vortex at the warning position is required as in a cold start. Rather, a continuing series of AMV-based FCDI analyses as often as every 15 min will be produced prior to, during, and following the Irma RI event. In this study, only the 6 h period with the first GOES-16 15 min AMVs will be examined with the FCDI and with the HWRF initialization, and then the 72 h forecasts with the COAMPS-TC and with the HWRF model, respectively, will be provided to illustrate the model performance during the Irma RI.

The methodology for this surface wind adjustment is described in Appendix A. It is noted that other satellite-based studies have utilized some methods to constrain the TC center position during the assimilation phase. For example, Minamide and Zhang (2018) [11] assimilated all-sky radiances from Himawari-8 in an ensemble Kalman filter initialization for Super-typhoon Soudelor (2015), and they imposed the MSLP at the pre-TC position every hour during the 6 h assimilation. Minamide and Zhang found that the assimilation of the infrared radiance improved not only the estimate of the initial intensity, but also improved the spatial distribution of the convective activity associated with the pre-Soudelor vortex. While the intensity variations in this study will emphasize the MSLP observations, the forcing here is wind vectors, and the MSLP solution is in response to that wind forcing. Although the six-hourly NHC best-track MSLP estimates could also be interpolated to 15 min values as an additional forcing term, that option will be examined in a future study.

Lewis et al. [6] provide only a brief description of the HWRF data assimilation that produced analyses to be discussed in Section 3. However, the Sawada et al. (2020) [12] article in this *Atmosphere*

special issue provides a detailed description of the two HWRF ensemble-variational hybrid data assimilation configurations using background error covariances from the global model ensemble forecast and the HWRF ensemble forecast. The key component related to this study is the HWRF vortex initialization (VI) step. The vortex-scale fields from the previous 6 h HWRF forecast are used when available (i.e., a warm start) as the first guess for the HWRF Domain 2 and Domain 3. However, the first-guess vortex is then adjusted based on the TC Vitals obtained from the appropriate TC warning center, which generally includes the fix position, MSLP, V_{max}, and wind radii. A second HWRF Data Assimilation System for generating the vortex structure and its environment on Domain 2 and Domain 3 is done over broader domains (28° × 28° and 15° × 15°) than the forecast domains. Finally, this HWRF Data Assimilation System analysis is merged or blended into the global model data assimilation analysis, except the increments below the 600 hPa pressure level are removed within 150 km radius of the TC center for hurricane intensity cases. In these cases, the AMV-related wind increments may be fully or partly eliminated within 300 km radius and below 400 hPa [11].

In the Lewis et al. [6] study that will be compared with the modified Elsberry et al. [1] FCDI analyses in Section 3, the HWRF initialization analysis was cycled each 6 h at the standard synoptic times (i.e., 00, 06, 12, and 18 UTC). It is noted that the FCDI analyses forced by the high temporal and spatial resolution GOES-16 AMVs will generate the full three-dimensional structure of the Irma vortex and its environment with a much less complex nudging approach that documents the evolution during the 6 h between standard synoptic times. The more complex HWRF initializations are designed to provide appropriate initial conditions for the HWRF model intensity predictions through at least 48 h because of the cycling ensemble assimilation across the synoptic time (i.e., incorporates observations both before and after the synoptic time, and its strong dependence on the vortex initialization step). However, these more accurate analyses are "snapshots" at six-hourly intervals that may not provide as detailed information on the Irma RI event timing, magnitude, and evolution that may be provided by the FCDI analyses each 15 min.

2.1.4. Simplified FCDI without Upscaling to NAVGEM

A unique aspect of the Elsberry et al. [1] approach was that the SAMURAI-COAMPS dynamic initialization analyses on the Domain 2 grid were also upscaled (or blended) to the Navy Global Environmental Model (NAVGEM) for its initial conditions rather than having to insert a synthetic vortex that was the practice in operations during the time of Hurricane Joaquin. This upscaling step effectively provides information regarding the high temporal and spatial resolution AMVs from the Domain 2 grid on the spatial resolution of the NAVGEM. In addition to improving the NAVGEM forecasts of track and intensity, the first 6 h of the NAVGEM forecast provided improved background and lateral boundary conditions for the next SAMURAI-COAMPS dynamic initialization (and now for the FCDI analysis).

The flow chart in Figure 3 summarizes the information flow between the NAVGEM and the FCDI prior to and following the assimilation of the 15 min GOES AMVs if the full Elsberry et al. [1] approach was to be utilized in this study. The first row items assume that a pre-TC circulation or Invest has been detected and a "cold-start" FCDI analysis at t − 6 h is required to begin the NAVGEM and the COAMPS-TC forecasts at t = 0 h, which will also be cold starts. The 4D Navy Data Assimilation System-Accelerated Representer (NAVDAS-AR) global analysis incorporating all available conventional and satellite observations within ± 3 h of t − 6 h is pulled from the archive. This NAVDAS-AR analysis will have had a synthetic TC vortex inserted as initial conditions for the NAVGEM forecast, which is also drawn from the archive. The next step along the first row in Figure 3 is to pull from the archives the COAMPS-TC cold start initial conditions, which includes an interpolation of the background and lateral boundary conditions for Domains 2 and 3. In addition, a TC bogus vortex (if available) will have been inserted in the spectrally smoothed fields (to represent the steering flow) of Domains 2 and 3. These cold-start COAMPS-TC are the initial conditions for the cold-start FCDI initial conditions at t − 6 h (right-most box in row 1 of Figure 3).

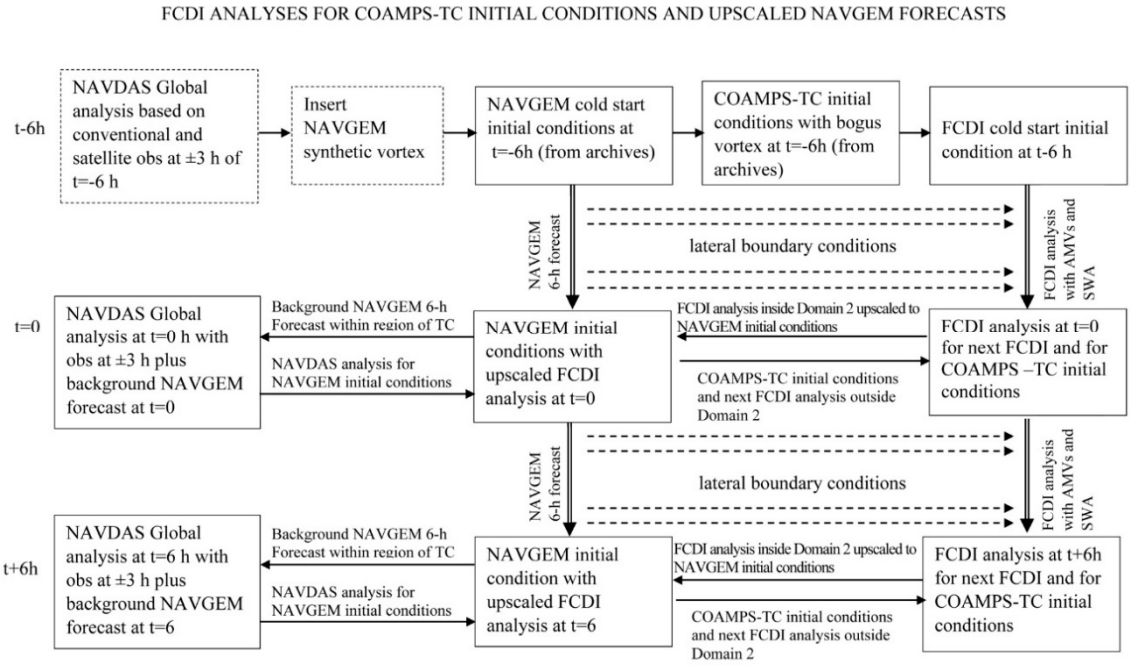

Figure 3. Flowchart of the full FCDI analysis procedure starting from six hours prior to the first detection of a pre-TC circulation so that the NAVGEM, the COAMPS-TC, and the FCDI are all cold starts. In this version that is similar to the Elsberry et al. (2018) [1] dynamic initialization, the FCDI analysis within Domain 2 at t = 0 h is upscaled to NAVGEM and is input to the NAVDAS-AR analysis, which is then downscaled to become the initial conditions outside of Domain 2 for the next FCDI analysis.

For this first cold-start FCDI, the initial conditions on Domains 1, 2, and 3 in Figure 2 are identical to the Control COAMPS-TC forecast that will be compared with the FCDI analyses during the first six hours. Two versions of the FCDI will be demonstrated in this study. In the first version (labeled as 15 min FCDI), the 15 min GOES-16 AMVs as in Figure 1b will be assimilated on Domains 2 and 3, and the GOES-13 hourly AMVs as in Figure 1a will be assimilated on Domain 1. In the second version labeled as hourly FCDI, only the hourly GOES-13 AMVs as in Figure 1a will be assimilated on all three domains. For the calculation of the FCDI wind increments with each new set of the 15 min AMVs relative to the COAMPS-TC model winds at the same time, those FCDI wind increments are held constant for the next 15 min of the COAMPS-TC dynamic initialization. If the next set of 15 min AMVs is missing, the same FCDI wind increments are held constant for another 15 min of COAMPS-TC dynamic initialization until a new set of 15 min AMVs is available. In the assimilation of the hourly AMVs, the t = 0 h FCDI wind increments in Equation (1) are the AMVs at t + 1 h minus model winds at t = 0 h. However, the t + 15 min FCDI wind increments are again based on the AMVs at t + 1 h, but it is now the model winds at t + 15 min that are subtracted from those AMVs. Similarly, the t + 30 (t + 45) minute FCDI wind increments are calculated by subtracting the model wind at t + 30 (t + 45) minutes. With this hourly FCDI methodology, the t = 0 wind increments will have the largest magnitude and lead on the largest adjustment of the model winds toward the t + 1 h AMVs, and then the t + 15 min FCDI wind increments will be much reduced compared to the t = 0 FCDI wind increments. Similarly, the t + 30 (t + 45) FCDI increments will be reduced compared to the t + 15 (t + 30) FCDI wind increments, and the adjustments of the model winds toward the t + 1 h AMVs will be progressively more gradual.

During the six-hour FCDI assimilation from the cold start at t − 6 h to the creation of the t = 0 FCDI analysis (Figure 3, upper-right corner), the surface wind adjustment is applied each 15 min as described in the Appendix A. The lateral boundary conditions for the fixed-in-space Domain 1 are provided by a NAVGEM six-hour integration from t − 6 h to t = 0 h, which is available from an archive so that the Control COAMPS-TC forecast can be later recreated for research studies such as this.

As described above, the unique aspect of the Elsberry et al. [1] approach was that the Domain 2 FCDI analysis is upscaled (blending coefficient equal to 1.0) to the NAVGEM initial conditions (middle row of Figure 3). That is, the next six hours of the FCDI from t = 0 h to t + 6 h will have background and lateral boundary conditions from a NAVGEM integration in which the NAVDAS-AR at t = 0 h input to the NAVGEM initial condition applies only outside of the Domain 2 solution from the t = 0 FCDI analysis, which is a warm start with no need for a bogus vortex in the initial conditions for a COAMPS-TC forecast from t = 0 h. Furthermore, if the surface wind adjustment has been successful such that the TC vortex center is close to the target six-hour position, there is no need for a vortex relocation. Since the COAMPS-TC model for the forecast is the same as is used in the FCDI, the model solution begins smoothly even as the nudging term is removed during the COAMPS-TC forecast from t = 0 h. When this FCDI analysis at t = 0 h, along with the NAVGEM initial conditions with that same upscaled FCDI analysis as indicated in the middle box of the second row in Figure 3, is the start of the next FCDI analysis, the first 15 min set of AMVs at t = 0 h will follow smoothly from the prior 15 min AMV set at t − 15 min. Since the model wind field at t = 0 h is the same as at the end of that last 15 min of the FCDI, the FCDI wind increments will evolve smoothly as the next FCDI analysis begins.

The lateral boundary conditions for Domain 1 during the next FCDI analysis from t = 0 h to t + 6 h (middle row in Figure 3) come from an integration of the NAVGEM, which would normally be from the first six hours of a 5–7 day forecast. However, the NAVGEM initial conditions in this technique now include the upscaled FCDI analysis within Domain 2, and thus a separate NAVGEM integration is required. Even for just a 6 h NAVGEM forecast, this is the most time-consuming component of the assimilation cycle. Because this NAVGEM integration is done on a separate computer than the first FCDI analysis, many file transfers are required, which is also time consuming.

The t + 6 h FCDI analysis procedure in the bottom row, third column of Figure 3 is similar to the t = 0 h FCDI analysis in the middle row. Each 15 min a new set of AMVs becomes available to calculate the FCDI wind increments relative to the corresponding 15 min model wind field as in Equation (1). For the surface wind adjustment calculation, the initial vortex position is the last TC position in the previous FCDI analysis and the target position is the t + 6 h fix by the warning center. Again, the FCDI analysis inside Domain 2 is upscaled (blended) to become part of the initial conditions for another 6 h NAVGEM integration that will provide the lateral boundary conditions for Domain 1 of the next FCDI analysis.

Recall that the primary objective of this study is to demonstrate the impact of first complete 6 h dataset of high-density GOES-16 AMVs on the FCDI analysis at 18 UTC 3 September. Although a 72 h COAMPS-TC forecast of the Irma RI event using that t = 0 h FCDI analysis as initial conditions will be another demonstration of the GOES-16 AMVs impact, the objective here is not to demonstrate any impact on the NAVGEM track and intensity forecasts as was the case in Elsberry et al. [1]. Furthermore, no SAMURAI wind increment analysis was done in Domain 1 in the Elsberry et al. [1] approach, and it was only the Domain 2 analysis (15 km) that was upscaled to the NAVGEM. Whereas that upscaling of the Domain 2 fields, and the separate 6 h NAVGEM global model integration, would slightly improve the deep layer steering flow for Irma, it will be assumed that improved steering would have little effect on the short-term environmental flow impacts of triggering the Irma RI event that is the focus of this study.

Thus, the fourth modification of the Elsberry et al. [1] approach has been to eliminate the upscaling of the Domain 2 fields to the NAVGEM, and thus eliminate the need for a separate 6 h NAVGEM integration to provide the Domain 1 lateral boundary conditions and updated Domain 1 fields (Figure 4). Rather, those lateral boundary conditions for Domain 1 will be provided from the archives. Furthermore, the FCDI will now be applied in Domain 1 utilizing the CIMSS hourly AMVs over all ocean areas that are included in Domain 1. Note that the Domain 2, which has the assimilation of 15 min AMVs, is now much larger (Figure 2). With the two-way integration in the FCDI now in Domain 1, and in a larger Domain 2, the impact of these GOES-16 AMVs will extend over a much larger area. Specifically, the AMVs in the larger Domain 2 will continually update areas in the

Domain 1 wind fields every 15 min that previously would have occurred via the 6 h NAVDAS-AR analysis and separate NAVGEM 6 h integration. The effects of the NAVDAS-AR global analyses outside Domain 1 will be transmitted inward via the archived NAVGEM lateral boundary conditions (Figure 4). Because the necessary NAVGEM files are available on the same computer as the FCDI is executed, it eliminates a large amount of file transfers between two computers. In combination with the elimination of the separate 6 h NAVGEM integration in Figure 3, the modified procedure in Figure 4 is much more efficient.

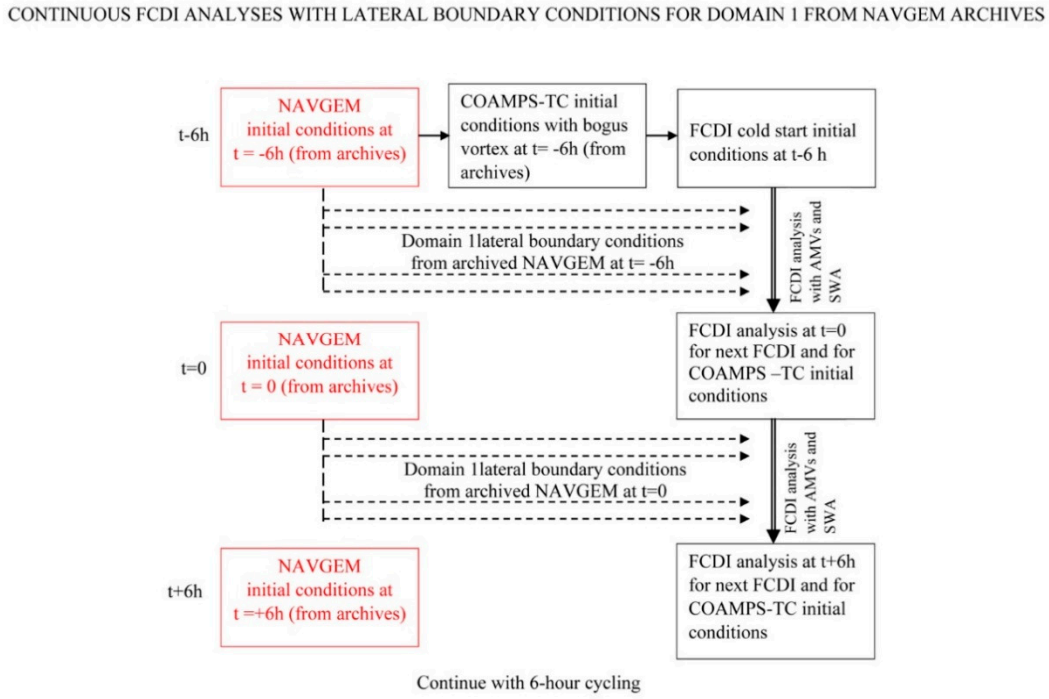

Figure 4. Flowchart as in Figure 3, except for the continuous six-hourly FCDI analyses as in this study in which the FCDI analysis within Domain 2 is not upscaled to NAVGEM. Rather, the archived NAVGEM fields each 6 h (red boxes) are used to provide the Domain 1 lateral boundary conditions for each FCDI analysis (dashed lines).

2.1.5. Summary of Modifications to the Elsberry et al. Approach

In summary, four modifications of the Elsberry et al. [1] dynamic initialization technique for assimilating high frequency (15 min) AMVs have been made to assimilate extremely high spatial resolution GOES-16 AMVs in the first 6 h period these AMVs were available prior to a RI event in Hurricane Irma. The first modification was to replace the SAMURAI subroutine calculation of the AMV-based increments with a Four-Dimensional Data Assimilation in which the raw AMV zonal and meridional wind components are inserted into the COAMPS-TC model for direct calculation of the nudging term in Equation (1). This is a straight-forward and efficient technique for assimilating the high temporal and spatial resolution GOES-16 AMVs reprocessed by CIMSS [7] without any thinning. The second modification has been to expand the sizes of Domains 2 and 3 (Figure 2) to encompass the areas of the high temporal (15 min) GOES-16 AMVs, and also to apply the FCDI technique in the oceanic areas of Domain 1 utilizing the special GOES-13 hourly AMVs, which had not been done in Elsberry et al. [1]. The third modification was to add a surface wind field adjustment in which a 300 km by 300 km and 1500 m deep layer centered on the TC position is used as a constraint on the regions of deep convection relative to the center, which then facilitates a connection between the boundary layer ascent with the cloud-top divergence inferred from the AMVs. Another objective of the continued adjustment of the surface wind field to move along the target pathway toward the known 6 h ending position such that the analyzed 6 h position is sufficiently close to the next warning position such that

the next assimilation cycle target position may then begin from the previous assimilation 6 h position with no vortex relocation or introduction of a bogus vortex being necessary. The Elsberry et al. [1] unique upscaling of the AMV-enhanced Domain 2 analysis to the NAVGEM to replace its synthetic vortex, and thereby improve its TC track and intensity forecasts, was not considered to be necessary for this study of the Irma RI event. Consequently, the upscaling of the FCDI analysis in Domain 2, and the separate 6 h NAVGEM forecast to provide the Domain 1 lateral boundary conditions for the next FCDI analysis, in the original flowchart (Figure 3) have been omitted in this study (Figure 4). This fourth modification of the Elsberry et al. [1] dynamic initialization technique provides a less complex and more time-efficient approach to demonstrate the impact of high temporal and spatial resolution GOES-16 AMVs on the FCDI analysis and 72 h forecast of the Irma RI event.

2.2. FCDI Analyses and COAMPS Forecasts of Irma RI Event

2.2.1. Characteristics of the Irma RI Event

Cangialosi et al. (2018) [5] is the official NHC report on Hurricane Irma, which was a noteworthy storm as it caused widespread devastation and was one of the strongest and costliest hurricanes on record in the Atlantic basin. Irma originated from a tropical wave that left the west coast of Africa on 27 August 2017. It became a hurricane at 0600 UTC 31 August only 30 h after it became a tropical depression, and attained major hurricane status by 0000 UTC 1 September, which was only two days after genesis. Unfortunately, the first RI of 70 kt increase over a 48 h period was when Irma was too far east in the Atlantic and not yet targeted by the GOES-16 meso scans so that no high temporal and spatial AMVs were available to study that first RI event.

Elsberry et al. [3] documented that the objective satellite consensus SATCON intensity estimates (Velden and Herndon 2020 [13]) at 30 min intervals were very useful in diagnosing the timing and magnitudes of two RIs and the two decays in Hurricane Joaquin. The SATCON intensities in terms of minimum sea-level pressure (MSLP) for Hurricane Irma are shown in Figure 5 (red line), and are compared with the NHC working best-track (WBT) intensities (thin black line) that are only available at 6 h synoptic times. Digital SATCON intensities are estimated to the nearest 1 mb and will be compared with the FCDI analyses. Particular attention will be given to the times of MSLP observations from the NOAA P-3 and Gulfstream-4 research aircraft and the Air Force Reserve reconnaissance aircraft (www.aoml.noaa.gov/hrd/Storm-pages/Irma2017/mission.html), which are in situ observations as the aircraft passed through the center (Figure 5, small black triangles).

For the SATCON versus NHC comparison of MSLP (Figure 5), the agreement is quite good during the first RI event that began late on 30 August and continued to midday on 31 August. However, large discrepancies between the two MSLP values exist during 1 September and 2 September, which is well before the first aircraft mission in Irma on 3 September that would have clarified which intensity was correct. The SATCON MSLP estimates decrease from 973 mb at 0745 UTC 1 September to 953 mb at 00 UTC 2 September when the NHC MSLP is ~966 mb. Whereas the SATCON remains near 953 mb until 12 UTC 2 September and later decreases to 950 mb at 21 UTC 2 September, the NHC MSLP increases to ~973 mb at 12 UTC 2 September, and then remains constant until 06 UTC 3 September. All of the individual satellite inputs to the SATCON indicate rising MSLPs after 00 UTC 3 September in association with an eyewall replacement cycle (ERC), but the timing of that steep MSLP rise varies among the member satellite estimates. The periodic ATMS sounder estimates (Figure 5, red triangles) have that steep rise at around 03 UTC 3 September. However, the 30 min ADT (blue dots) that is derived from high spatial and temporal resolution GOES-16 imagery maintains the MSLP at 955 mb until 12 UTC, and then has an 8 mb rise in 2 h. The SATCON goes down the middle of these rising MSLP estimates. At 0915 UTC 3 September when the CIMSS began the high temporal (15 min) resolution AMVs, the SATCON MSLP estimate is ~965 mb, but is still rising rapidly. At the first synoptic time (12 UTC) after the beginning of the high-density GOES-16 AMVs, the NHC WBT and the SATCON both have the MSLP ~970 mb, but this is the beginning of the Irma RI event in the NHC WBT while the

SATCON MSLP is still rising. A microwave image at 16 UTC 3 September (not shown) indicates that Irma has a broader eye than at 09 UTC, and suggests an eyewall replacement cycle may be underway consistent with rising MSLP.

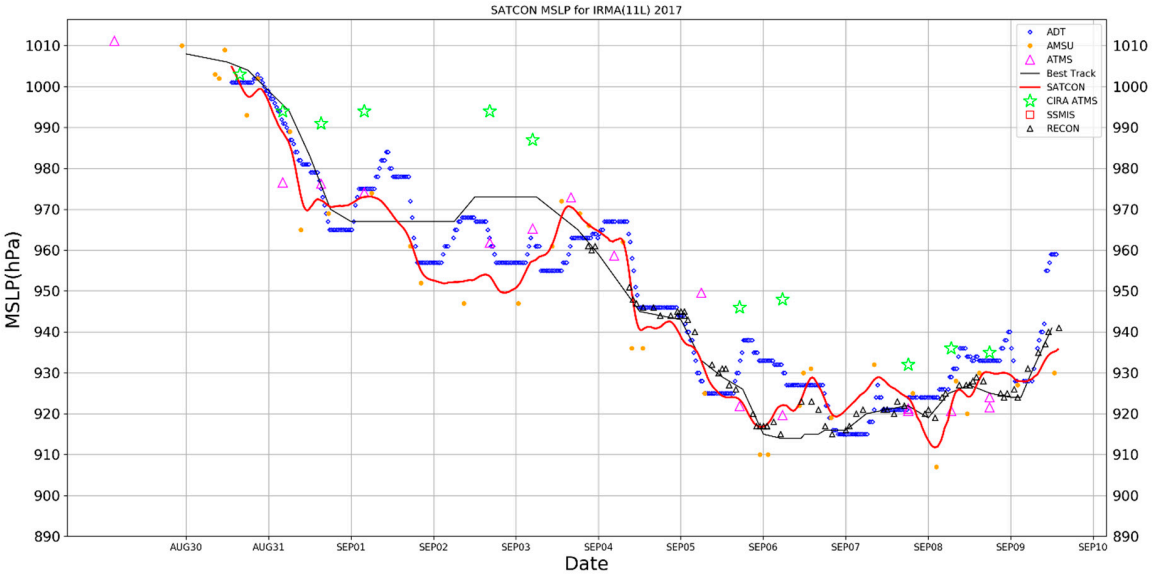

Figure 5. Real-time CIMSS tropical cyclone SATCON minimum sea-level pressure (MSLP, hPa) estimates at 30 min intervals (red line) from 0000 UTC 30 August 2017 to 1200 UTC 9 September for Hurricane Irma that incorporate various satellite instruments (see inset in upper right) and include the aircraft recon observations (small, black triangles) and the six-hourly NHC working best-track intensity estimates digitized to 5 kt increments (thin black line).

As indicated in Figures 3 and 4, the FCDI analyses begin from a cold start of the COAMPS-TC initial conditions at a synoptic time, and these initial conditions contain a bogus vortex based on the TC Vitals. Note that this COAMPS-TC bogus vortex is based on the NHC maximum wind estimate, and the MSLP solved from a balance equation will not necessarily be equal to the NHC MSLP estimate, but the HWRF vortex initialization step in Lewis et al. [6] is designed to be able to match the NHC MSLP estimate as well. Although an ambiguity exists between the SATCON and the NHC WBT intensity estimates at 12 UTC 3 September, in order to facilitate a comparison between the FCDI dynamic initialization and the Lewis et al. [6] HWRF initialization with the same GOES-16 AMV dataset, the FCDI will begin from 12 UTC 3 September. A 6 h FCDI dynamic initialization to 18 UTC 3 September will be compared in Section 3 with the Lewis et al. [6] HWRF initialization centered on the 18 UTC 3 September synoptic time.

Based on both the SATCON and the NHC WBT intensity changes in Figure 5, four stages of the Irma RI may be defined that are well supported by aircraft MSLP observations: (i) the pre-extreme RI stage; (ii) the extreme RI stage; (iii) the intermediate constant-intensity stage; and (iv) the extended slower RI stage. The NHC pre-extreme stage is defined to begin at 12 UTC 3 September and end with the first NOAA P-3 aircraft MSLP observations in Irma, which were at ~21–22 UTC 3 September (see small, black triangles) with magnitudes near 961 mb. As described above, the NHC MSLP is also 961 mb because such aircraft observations are considered to be highly accurate. Thus, the NHC MSLP evolution is a linear decrease from 967 mb at 12 UTC to 961 mb at 21–23 UTC 3 September. By contrast, the SATCON pre-extreme RI stage is defined to begin at 12 UTC 3 September have a linear decrease from 970 mb to 963 mb at ~04 UTC 4 September, and then have constant MSLP to ~08 UTC 4 September just prior to the extreme RI event according to the SATCON (Figure 5). Note that the SATCON MSLP is slightly high (~5 mb) at the time of the first NOAA aircraft observations.

Because the NHC file is at 6 h synoptic times, the first segment of this RI event that is designated as extreme RI begins with MSLP = 961 mb at 06 UTC 4 September and ends with 944 mb at 12 UTC 4 September, which is a linear 17 mb decrease in 6 h that is defined by two aircraft mission sets of MSLP observations (Figure 5, small black triangles). According to the real-time SATCON file, this extreme RI stage begins with MSLP = 962 mb at 0815 UTC and ends with 942 mb at 1045 UTC, which is a 20 mb decrease in only 2.5 h. Thus, the extreme nature of this RI event in Hurricane Irma is better revealed in these SATCON estimates that are not constrained to begin or end on a 6 h synoptic time.

Multiple aircraft MSLP observations during 12 UTC 4 September to 00 UTC 5 September (small, black triangles in Figure 5) document that the MSLP was nearly constant within +/−2 mb during the intermediate constant-intensity stage. Indeed, seven aircraft MSLP observations within +/−2 h of 00 UTC 5 September document the ending of this constant-intensity stage before the start of the second segment of the RI event. Consequently, the NHC MSLP values vary linearly from ~945 mb at 12 UTC 4 September to ~943 mb at 00 UTC 5 September. Almost all of the 30 min SATCON MSLP estimates from 1145 UTC to 1915 UTC 4 September are within ± 1 mb of 942 mb, which certainly supports the existence of this intermediate constant-intensity stage in Irma.

The first segment of the RI event that is interrupted by this short constant-intensity stage, and then followed by an extended slower RI segment, may not seem important relative to the overall RI event during which the intensity increased from 100 to 155 kt. However, the objective of improved understanding of all four stages of this Irma RI event requires understanding of how the environmental factors or the internal physical processes contributed also during the pre-extreme RI segment, and later contributed to an interruption of the extreme RI stage. Fischer et al. (2020) [14] have extensively analyzed the NOAA and Air Force aircraft datasets in Irma, and have concluded the Irma RI event was comprised of two rapidly evolving eyewall replacement cycle (ERC) episodes that each completed in less than 12 h. Flight-level and dropwindsonde observations from multiple center overpasses by each aircraft, and with the tail Doppler radars on the NOAA aircraft, allowed Fischer et al. [14] to construct axisymmetric vortex structure plots for each mission. They propose that the two ERC episodes appear to be linked to how the Irma vortex responded to changing environmental conditions that they estimated from the Statistical Hurricane Intensity Prediction Scheme (SHIPS; De Maria and Kaplan 1994) [15]. In a future study, we will compare the FCDI three-dimensional analyses of the Irma vortex at the same times as the Fischer et al. [14] aircraft-based axisymmetric vortex analyses, and compare the continuous (15 min) FCDI-analyzed environmental conditions with the six-hourly SHIPS-based environmental conditions.

Although there were two 6 h gaps between the three clusters of aircraft MSLP observations between 00 UTC 5 September and 00 UTC 6 September (Figure 5), these aircraft observations document the last RI stage that intensified somewhat slower for an extended period. The SATCON MSLP decrease for this extended slower RI stage begins from 943 mb at 2045 UTC 4 September and continues steadily to a minimum of 915 mb at 0115 UTC 5 September. Note again that neither the starting time nor the ending time is at a 6 h synoptic time. While the NHC WBT has a slower deepening rate for a short period during this stage, the aircraft observations tie down the 915 mb MSLP at 00 UTC 6 September.

As will be demonstrated in Section 3 below, the post-season, best-track MSLP evolution is a smoothed version of the WBT MSLP values in Figure 5. Rather than having a constant MSLP stage as in the WBT and the SATCON, the intermediate 12 h period is portrayed as a 7 mb decrease between the previous and the subsequent 6 h periods that have MSLP decreases exceeding 12 mb (Cangialosi, et al. [5], their Table 1).

2.2.2. AMV-Based FCDI Analyses for Initialization

As indicated in Figures 3 and 4, the first FCDI analysis is a cold start from the COAMPS-TC initial conditions (also a cold start) at 12 UTC 3 September (Figure 6), which is the first synoptic time after the 15 min GOES-16 AMV data became available at 0915 UTC 3 September (Figure 1b). The FCDI analyses at z = 12,860 m will be described first because it is primarily the cloud-top AMVs that are available

above Hurricane Irma, which had an intensity of 100 kt at 12 UTC 3 September according to the NHC best track [5]. As Irma is to the south of a strong ridge to the north, the primary outflow is toward the west and southwest (Figure 6a). Note that northerly environmental flow is impinging on the Irma outflow to the northeast of the center, which contributes to the vertical wind shear.

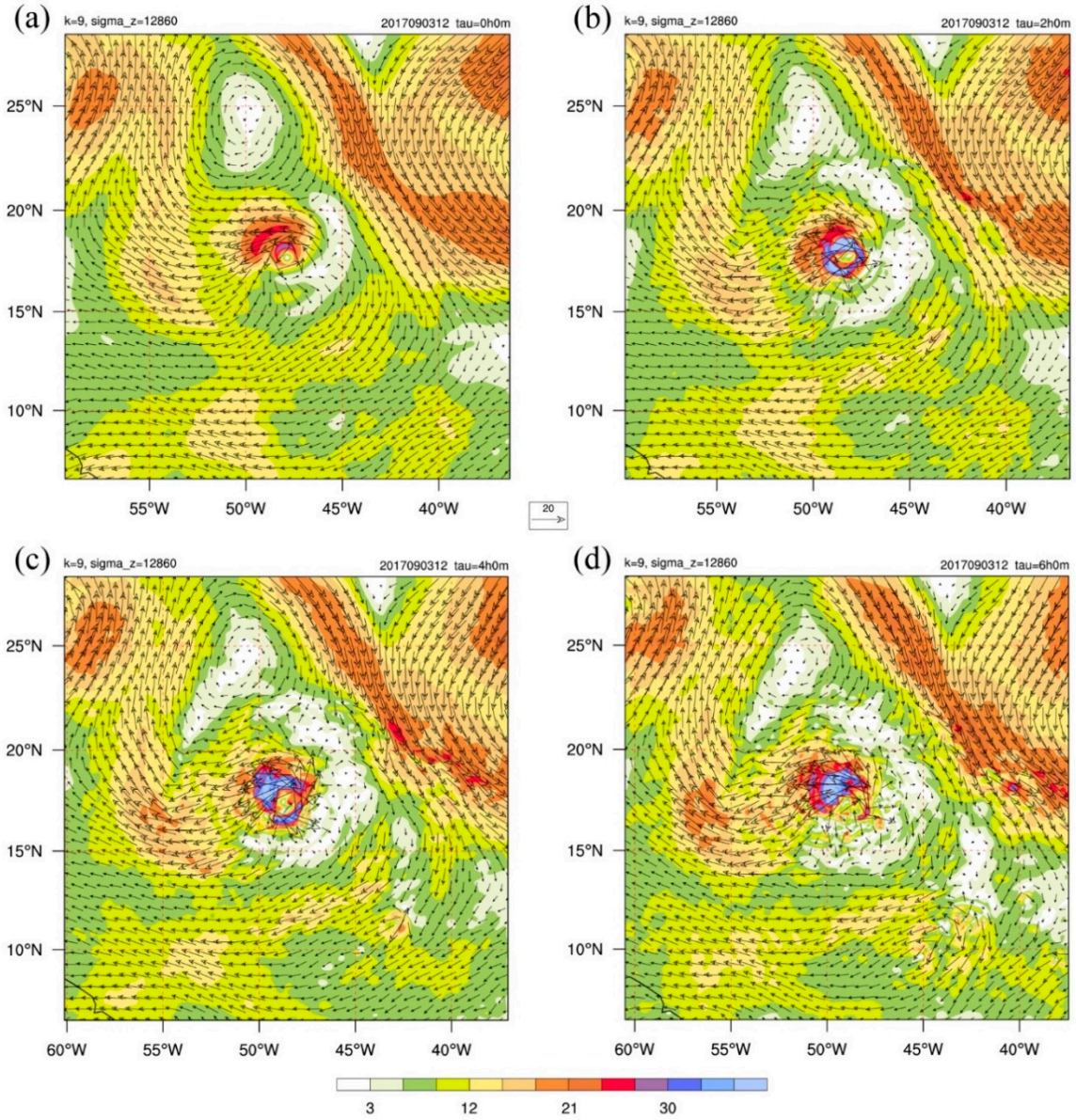

Figure 6. Domain 3 FCDI analyses of z = 12,860 m wind vectors (m s^{-1}; color bar at bottom and 20 m s^{-1} length indicated by arrow in middle) starting from cold-start COAMPS-TC wind vectors in panel (**a**) and then 15 min AMV-based FCDI analyses at (**b**) tau = 2 h, (**c**) tau = 4 h, and (**d**) tau = 6 h.

The FCDI wind increments relative to that COAMPS-TC cold-start z = 12,860 m analysis (Figure 6a), which is also the Control initial conditions, are shown in Figure 7a. The most notable feature in these FCDI wind increments is the extensive east-west band of wind increments along 20° N that are directed toward the north-northeast with magnitudes as large as 6.5 m s^{-1}. The interpretation is that the 15 min AMVs are indicating that there is actually outflow in a region that the Control has inflow vectors impinging on the Irma outflow (Figure 6a). The AMVs are also indicating an extensive east-west orientated convergence area to the south of the Irma center, and localized areas of stronger outflow toward the northeast near 19° N, 44° W and toward the southwest near 17° N, 51° W.

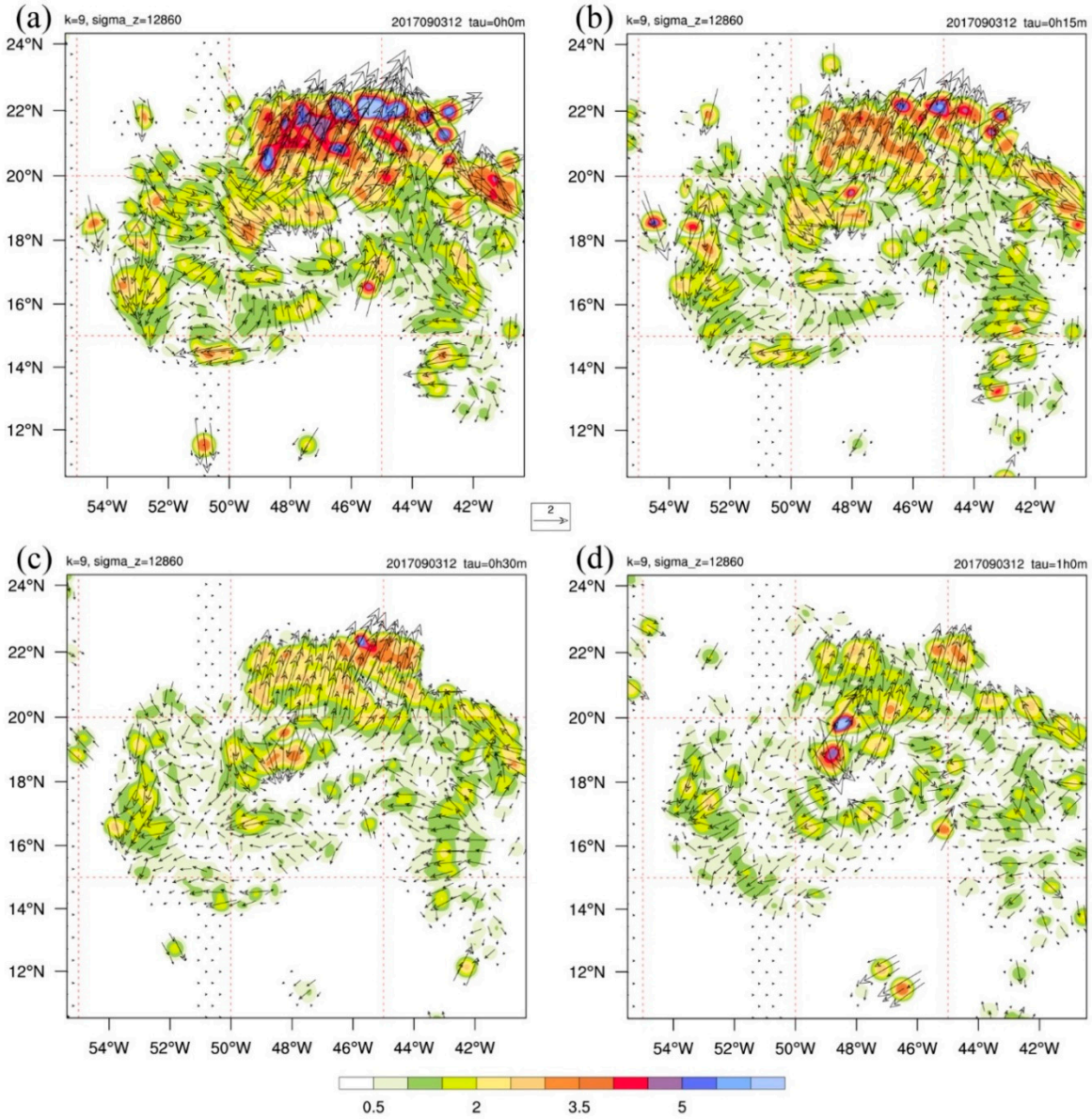

Figure 7. As in Figure 6, except for the 15 min AMV-based FCDI wind increments (m s^{-1}; color bar at bottom and 2 m s^{-1} vector magnitude indicated by arrow in middle) at (**a**) tau = 0 h, (**b**) tau = 15 min, (**c**) tau = 30 min, and (**d**) tau = 1 h.

Just 15 min later (Figure 7b), the FCDI wind increments have the same pattern, but the magnitudes have decreased. This reduction in magnitudes indicates that the model wind fields are already being nudged toward the AMVs. After another 15 min (Figure 7c), the wind increment magnitudes have been further reduced, and the areas with larger wind increments have shrunk in size. The area to the north along 20° N continues to have the largest magnitude (3–5 m s^{-1}) outflows against the impinging northerly vectors in the Control (Figure 6a). Nevertheless, there are also large areas to the south and southwest of the center that now have FCDI wind increments that are less than 1 m s^{-1}. After one hour of nudging these FCDI wind increments (Figure 7d), there are still wind increments at the z = 12,860 m indicating the AMVs have larger outflows than the model wind vectors (e.g., toward the north along 20° N and toward the southwest in the area between 15° N–18° N and 50° W–52° W). However, there are two highly localized areas of large magnitude (~5 m s^{-1}) FCDI wind increments near 18° N, 48° W that may be indicating deep convection in response to the stronger upper-level outflows over the past hour.

Comparing the FCDI z = 12,860 m analysis at tau = 2 h (i.e., 14 UTC 3 September) in Figure 6b with the Control analysis in Figure 6a illustrates how the nudging of eight sets of 15 min AMVs has modified the Irma vortex wind field plus the near-environment flow. The blue ring around the center in Figure 6b indicates a stronger outflow (>30 m s^{-1}) in all quadrants, but especially outflow toward the northeast and north in the regions with the largest FCDI wind increments in Figure 7a–c. Indeed, the northerly environmental flow on the east side of the ridge to the north of Irma no longer impinges on the outflow; rather, there is an extensive region of near-zero wind vectors between the northerly environmental flow and the Irma outflow. The strong almost-radial outflow to the west of the center continues some distance before turning anticyclonically to move poleward in advance of the upper-tropospheric trough well to the northwest of the center.

At tau = 4 h (i.e., 16 UTC 3 September) in Figure 6c, the magnitudes of the outflow vectors in the northwest quadrant exceed 30 m s^{-1} and extend ~200 km from the center. The outflow in that quadrant has a cyclonic curvature that quickly turns anticyclonic and then farther west turns poleward in advance of the upper-tropospheric trough. At tau = 6 h (i.e., 18 UTC 3 September) in Figure 6d, the outflow has become even more asymmetric with no outflow toward the south. The high-speed outflow in the northwest quadrant has extended farther to the west of the center. With just six hours of the GOES-16 AMVs as in Figure 1b, not only has the upper-level vortex outflow greatly changed, the near-environment flow has also been substantially modified. This highly asymmetric upper-level vortex is then the "warm start" for the 72 h COAMPS-TC forecast rather than an idealized bogus vortex in a cold start as in Figure 6a.

One of the subtle impacts of the FCDI wind increments is to modify the outflow from an intense, almost-point vortex that becomes evident near 11° N, 43° W in Figure 6c. These isolated vortices that are vertically oriented are occasionally predicted by the COAMPS-TC at low latitudes well away from the developing vortex center, and because they intensify quickly, the TC vortex tracker may suddenly switch to that center hundreds of kilometers away. Although the nudging of the AMV-based FCDI wind increments does not completely eliminate the outflow from the isolated vortex, the upper-level flow is deflected around its outflow in Figure 6d.

Another demonstration of the impact of 15 min AMVs in the tau = 6 h (Figure 6d) is to compare with the 6 h COAMPS-TC forecast (Figure 8a) from the same cold-start initial conditions in Figure 6a. Note that the inner-core outflow in Figure 8a is similarly asymmetric with >30 m s^{-1} vectors in an area extending to the north-northwest of the center. However, this 18 UTC 3 September COAMPS-TC forecast has the northerly environmental flow impinging on the outflow in the northeast quadrant just as in the 12 UTC 3 September initial conditions in Figure 6a. By contrast, the FCDI analysis in Figure 6d has a broad band of near-zero winds between the outflow in the northeast quadrant and the northerly environmental flow. Consequently, that band of strong northwesterly environmental flow farther to the east has been weakened and displaced to east compared to the same band in Figure 8a. Whereas the FCDI analysis also has strong outflow from the entire western semi-circle, the COAMPS-TC forecast has almost no outflow in the southwest quadrant. Clearly, the assimilation of the high temporal and spatial resolution GOES-16 AMVs in the 6 h FCDI dynamic initialization between 12 UTC and 18 UTC have had a large impact on the vortex-scale outflow magnitude and direction as well as on the adjacent environmental flow within ~500 km of the center.

The FCDI analyses at z = 12,860 m when hourly GOES-13 AMVs are incorporated instead of 15 min GOES-16 AMVs are displayed in Supplementary Figure S1. The FCDI wind increments (similar to Figure 7) for these hourly AMVs are presented in Figure S2. Since these hourly AMVs are missing the high-density AMVs in the upper troposphere as in Figure 1b near the center, these FCDI wind increments are only available at outer radii and in the environment. Nevertheless, there are still FCDI z = 12,860 m wind increments of ~5 m s^{-1} at the tau = 0 h (Figure S2a) when there are hourly AMVs with magnitudes and/or directions that deviate from the cold-start COAMPS-TC winds at tau = 0 in Figure S1a. At tau = 15 min (Figure S2b), the FCDI wind increments have been further nudged toward the hourly AMVs at tau = 1 h. The tau = 2 h (and 4 h) FCDI analysis in Figure S1b

(Figure S1c) display the effects of the hourly AMV nudging. Note that the hourly FCDI analysis at 18 UTC 3 September (Figure S1d) more closely resembles the 6 h COAMPS-TC forecast (Figure 8a) near the center. Furthermore, the northerly environmental flow is impinging on the hourly FCDI analysis outflow just as in that 6 h COAMPS-TC forecast because no hourly AMVs were available near the center. On the other hand, the concentration of hourly AMVs to the west and northwest of the center leads to the hourly FCDI analysis of the Irma outflow having a similar impact on the environmental flow to the west as in the 15 min FCDI analysis in Figure 6d.

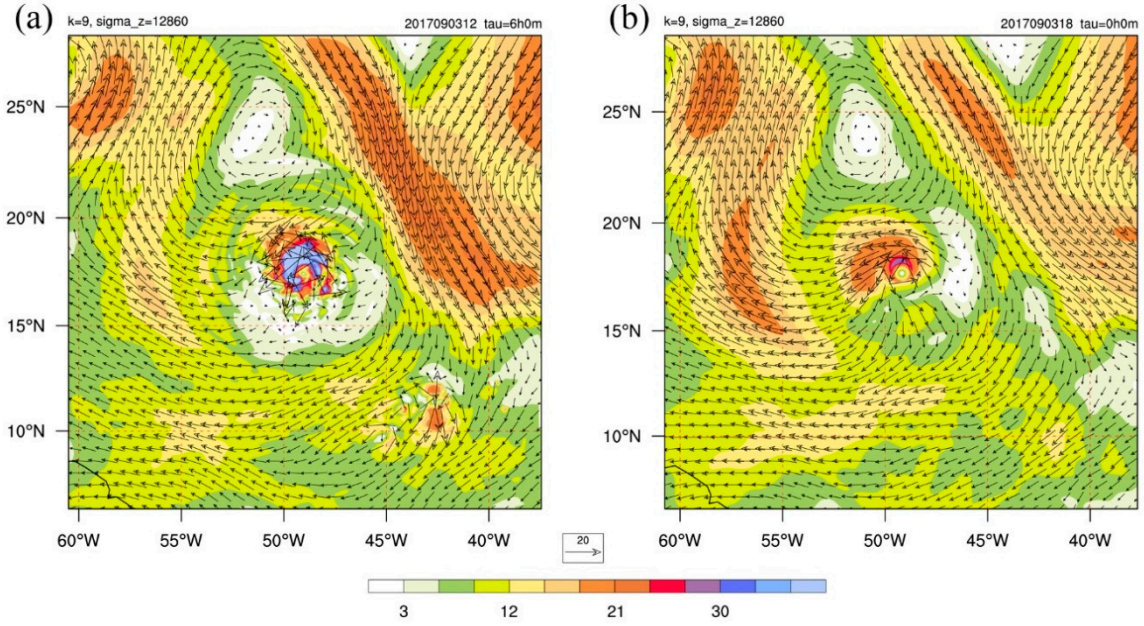

Figure 8. Domain 3 z = 12,860 m wind vectors (m s^{-1}, color bar and 20 m s^{-1} length indicated by arrow at bottom) at 18 UTC 3 September from (**a**) six-hour COAMPS-TC forecast from cold-start initial conditions in Figure 6a that might be used as warm-start initial conditions versus (**b**) the cold-start initial conditions with a bogus vortex that are actually used for Control 72 h forecast.

The differences in the 15 min AMV-based FCDI analyses at z = 300 m elevation (Figure 9b) relative to the COAMPS-TC initializations are subtler than at z = 12,860 m (Figure 6). The cold-start COAMPS-TC initial conditions at 12 UTC 3 September (Figure 9a) have a broad low-level vortex with the Radius of Maximum Wind (RMW) at approximately 35 km, a secondary maximum at 160 km to the north of the center, and the Radius of 18 m s^{-1} (R18) is at approximately 500 km to the north of the center. The 6 h COAMPS-TC forecast z = 300 m winds at 18 UTC 3 September that might be an alternative for a warm-start 72 h COAMPS-TC forecast are shown in Figure 9c. This z = 300 m vortex is more symmetric with the same RMW = 35 km, but no secondary maximum. This vortex is slightly more compact than in Figure 9a with a R18 ≈ 410 km on the north side. By contrast, the six-hour, 15 min AMV FCDI analysis vortex at z = 300 m (Figure 9b) is asymmetric and resembles the cold-start COAMPS-TC initial conditions in Figure 9a, which is not unexpected since those initial conditions were the background flow in the surface wind adjustment that was translated along the target pathway (Appendix A). However, the 15 min FCDI vortex is slightly more compact with a RMW ≈ 30 km and the R18 ≈ 355 km to the north. Similarly, the hourly AMV FCDI analysis vortex (Figure 9d) is asymmetric and also resembles those initial conditions that the surface wind adjustment has moved along the target pathway. The hourly FCDI vortex is slightly more broad (RMW ≈ 40 km, R18 ≈ 375 km) than the 15 min AMV FCDI vortex.

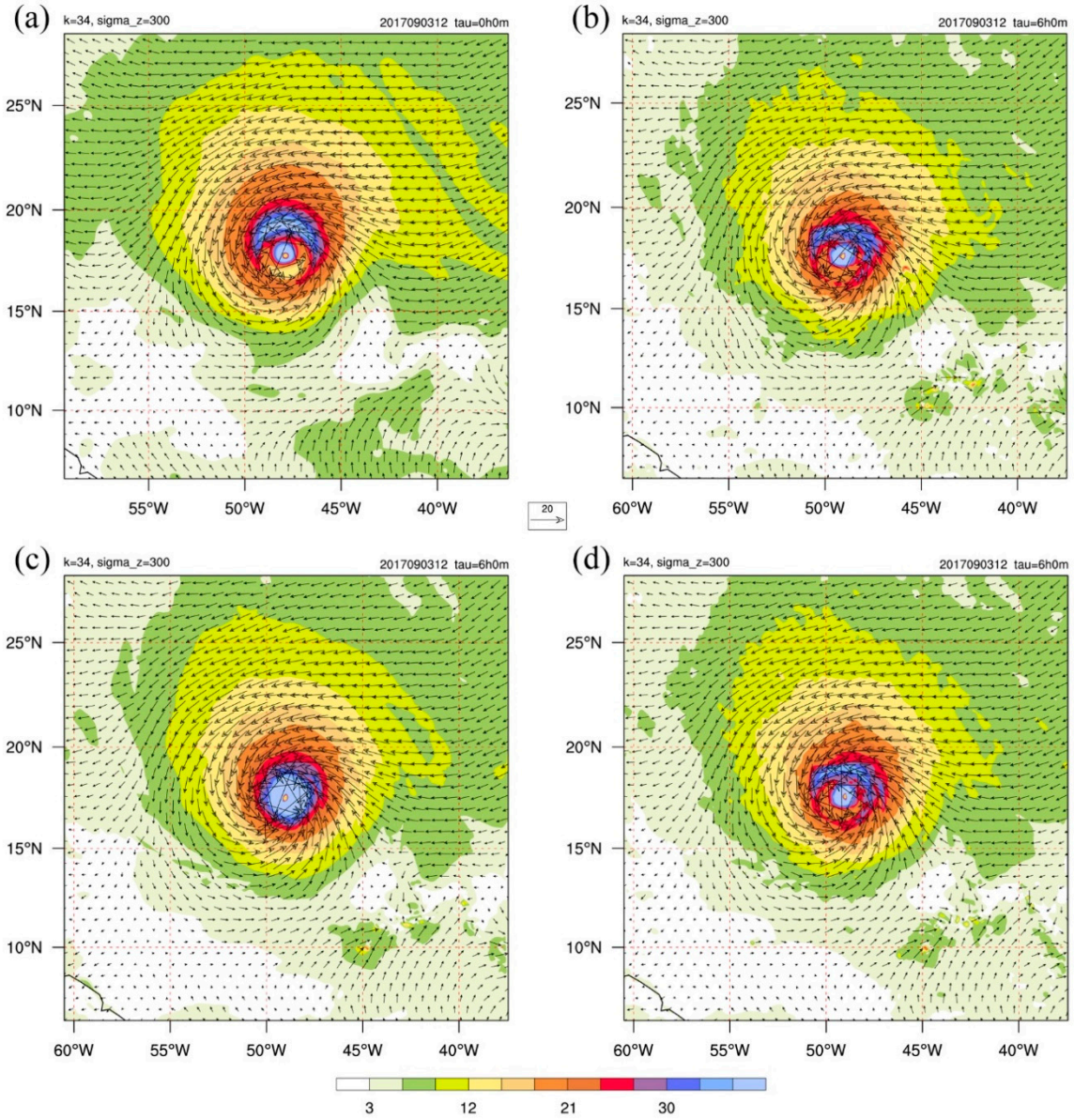

Figure 9. Domain 3 z = 300 m wind vectors (m s^{-1}; color bar at bottom and 20 m s^{-1} length indicated by arrow in middle) starting from cold-start COAMPS-TC wind vectors at 12 UTC 3 September in panel (**a**) and then the 15 min AMV and hourly AMV FCDI analyses after 6 h (18 UTC 3 September) in panels (**b**) and (**d**). The COAMPS-TC forecast from initial conditions in panel (**a**) after 6 h in panel (**c**).

More detailed descriptions of the Irma inner-core 300 m wind fields as in Figure 9 are displayed in Figure S3. The effect of the symmetric bogus vortex flow for the Control (cold-start) COAMPS-TC at 12 UTC 3 September is evident in Figure S3a. The six-hour COAMPS-TC forecast Figure S3e from these initial conditions has a stronger (>54 m s^{-1}) and broader RMV region, and especially in the northwest quadrant. Much stronger winds exist in the southern semicircle where a minimum of <15 m s^{-1} near 17° N in Figure S3a has been replaced with wind speeds ≈ 45 m s^{-1} (Figure S3c). The six-hour z = 300 m FCDI analysis that has assimilated the 15 min GOES-16 AMVs (which are primarily at the cirrus level) is displayed in Figure S3b. Two RMWs > 54 m s^{-1} are analyzed, with the RMV almost directly east of the center at ~16 km radius and the maximum to the southwest at ~25 km radius. Thus, the inner-core z = 300 m wind field is analyzed to be highly asymmetric due to the incorporation of the 15 min AMVs. Perhaps surprisingly because the hourly GOES-13 AMVs as in Figure 1a do not have dense coverage above the inner core, nevertheless the six hours of assimilating those hourly AMVs (Figure S3d) have

resulted in a similar highly asymmetric isotach distribution as did the 15 min AMVs (Figure S3b). The tentative explanation is that the environmental flow on a larger scale than the inner core may also contribute to an asymmetric inner-core vortex structure within the boundary layer of an intense TC.

For both the 15 min AMV FCDI analyses (Figures 6d and 9b) and the hourly AMV FCDI analyses (Figure S1d and Figure 9d) at 18 UTC 3 September, these become the warm-start initial conditions for the 72 h COAMPS-TC forecasts. That is, the upper-tropospheric wind field has been nudged to be consistent with the 15 min or the hourly AMVs, the mass field has been adjusted to the FCDI wind increments, and the dynamic, thermodynamic, and moisture processes of the COAMPS in the FCDI are the same as in COAMPS-TC forecast model. To avoid a vortex relocation step, the 6 h FCDI analyses should be within the position fix errors, which is the objective of the surface wind adjustment that has a target path from the t = 0 h position to the t = 6 h fix position that is applied each 15 min at the times of new AMV datasets (Figure 10a, pink dots). For both the 15 min AMV FCDI (blue dots) and the hourly AMV FCDI (green dots), the ending 6 h position is along the target path, but is slow by 40–45 min (~20 km) of target path ending position. Note that the target path for the next FCDI analysis will start at these 15 min AMV FCDI or hourly AMV FCDI ending points, so there is no vortex relocation required. The 6 h COAMPS-TC forecast track (Figure 10a, gold dots) has had some deviations from the target path and is slightly farther from the target path ending point.

It is emphasized that the Control COAMPS-TC 72 h forecast will be another cold start in which a bogus vortex is placed at the fix point, the wind field is specified to fit the TC Vitals, and the mass field is derived from a dynamic balance equation. As shown in Figure 8b, this new vortex wind structure at z = 12,860 m is quite different from the 6 h COAMPS-TC forecast vortex wind structure in Figure 8a. Although the corresponding warm-start FCDI vortex at 18 UTC 3 September will not necessarily have the V_{max} or the MSLP in the TC Vitals at that time, these two intensity measures of the FCDI vortex are self-consistent and representative of the AMV divergence/convergence forcing. Furthermore, the horizontal and vertical wind structure in the FCDI vortex should be representative of the mesoscale distribution of convective heating. The surface wind adjustment has been demonstrated to be successful in translating the vortex close to the desired target (fix) position. However, the dependence of the 15 min AMV FCDI vortex at z = 300 m after 6 h (Figure 9b) and the hourly AMV FCDI vortex at z = 300 m after 6 h (Figure 9d) on the COAMPS-TC vortex in the cold-start initial conditions (Figure 9a) could be a benefit or a degradation depending on how accurate those COAMPS-TC initial conditions are in this cold-start situation.

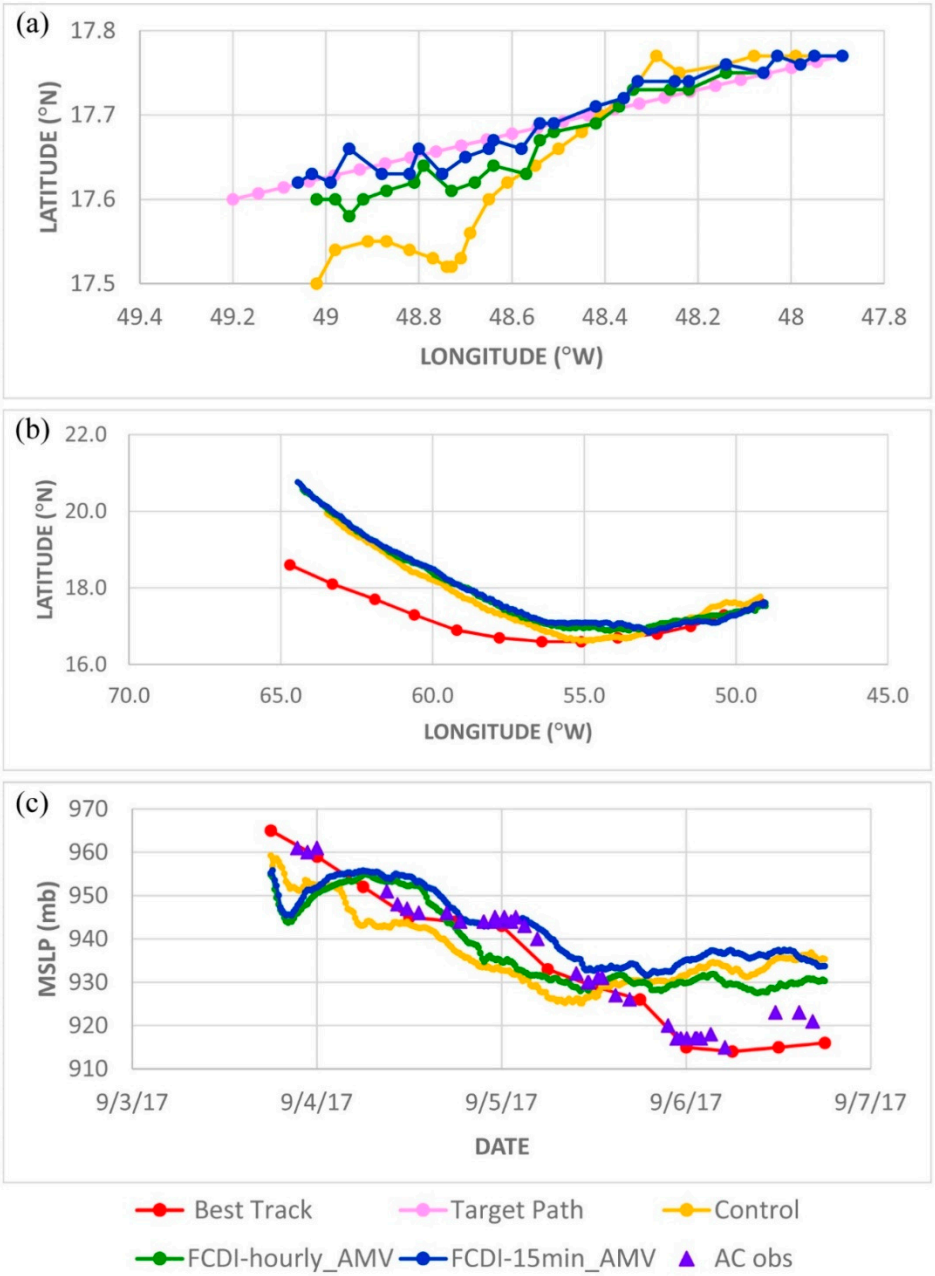

Figure 10. (**a**) Six-hour FCDI surface wind adjustment target path each 15 min (pink dots) starting from 17.77° N, 47.9° W position at 12 UTC 3 September and ending at Irma best-track position 17.6° N, 49.2° W at 18 UTC 3 September, and then corresponding 15 min positions for six-hour Control COAMPS-TC forecast (gold dots) and for FCDI vortex positions based on 15 min AMVs (blue dots) and based on hourly AMVs (green dots). (**b**) Irma best-track positions each six hours from 18 UTC 3 September to the 18 UTC 6 September ending at 18.6° N, 64.7° W compared to COAMPS-TC forecast positions of Control (19.95° N, 63.48° W, gold dots), 15 min AMV FCDI at 20.76° N, 64.44° W (blue dots), and hourly AMV FCDI at 20.57° N, 64.29° W, green dots). (**c**) Irma best-track MSLP (mb) each 6 h (red dots) starting from 18 UTC 3 September to 18 UTC 6 September compared with COAMPS-TC MSLP forecast at 15 min intervals by Control (gold dots), 15 min AMV FCDI (blue dots) and hourly AMV FCDI (green dots). Note that NOAA and Air Force aircraft MSLP observations are indicated by purple triangles.

2.2.3. COAMPS-TC Forecasts from AMV-Based FCDI Analyses

The 72 h COAMPS-TC forecasts from 18 UTC 3 September by the Control, the hourly AMV-based FCDI analysis, and the 15 min AMV-based FCDI analysis are compared with the NHC best track

in Figure 10b. As indicated above, this Control COAMPS-TC forecast is from the Figure 8b initial conditions and has a bogus vortex based on the TC Vitals position, intensity, and vortex structure at 18 UTC. Although this Control track forecast has some oscillations in the first 8 h, this Control has the better path forecast at 24 h and 30 h. This Control then has a similar (but slower) path as the COAMPS-TC forecast as the hourly AMV FCDI and 15 min AMV FCDI analyses, which start from the FCDI ending positions in Figure 8a. Because these FCDI analyses had the surface wind adjustment procedure each vortex was being translated down the correct path at tau = 6 h, and while the corresponding 72 h COAMPS-TC track forecasts initially had a better track forecast than the Control, other factors contribute to an erroneous turn more to the north than the NHC best track. In the future, these FCDI-based COAMPS-TC track forecasts will be repeated with the upscaling of the FCDI Domain 2 fields to NAVGEM as in Figure 3 to determine whether that procedure will reduce the FCDI track forecast errors at the larger forecast intervals.

The corresponding 72 h COAMPS-TC intensity forecasts from 18 UTC 3 September for the Control, the hourly AMV FCDI analysis, and the 15 min AMV FCDI analysis are provided in Figure 10c. Note that the NOAA and Air Force Reserve aircraft MSLP observations are displayed as in the SATCOM intensity plot in Figure 5. Both the Control and the two FCDI-based COAMPS-TC intensity forecasts begin with MSLPs that are 8–10 mb below the NHC initial WBT value. Most importantly, all three COAMPS-TC forecasts predict an immediate rapid deepening instead of rising (or at least near-constant) MSLP as in the SATCON intensity (Figure 5). Recall from Figure 6d, and also from Supplementary Figure S1d, that the cloud-top AMVs over the Irma vortex are consistent with large outflow aloft. The proposed explanation is that the TC Vitals that were used to define the cold-start COAMPS-TC and the cold-start FCDI at 12 UTC 3 September had a MSLP (namely the NHC WBT) that was too high. Specifically, the more likely MSLP (even at 18 UTC 3 September for the Control) based on the ADT values in Figure 5 is much lower. A future study will examine whether initialization of the FCDI analyses and the COAMPS-TC with MSLPs consistent with the SATCON will provide a more consistent intensity evolution during the pre-extreme RI stage.

Ignoring for now the first ~15 h (9 h) of the two FCDI (Control) intensity forecasts in Figure 10c as being the adjustment period to the initial conditions, the NHC post-season best-track MSLP is continuing a rapid decrease from 952 mb at 06 UTC 4 September to 945 mb at 12 UTC. However, then the MSLP decrease is only 2–3 mb over the next 12 h, which corresponds to the intermediate constant-intensity stage defined above. The Control COAMPS-TC forecast (Figure 10c, gold dots) has a rapid MSLP decrease from 954 mb at 03 UTC 4 September to 943 mb at 06 UTC, and then has a 6 h constant-intensity stage before beginning the second rapid MSLP decrease. Thus, the Control forecast misses (or optimistically, just has the wrong timing of) the intermediate constant-intensity stage between 18 UTC 4 September and 03 UTC 5 September according to the aircraft observations.

The 15 min FCDI-based and hourly FCDI-based COAMPS-TC intensity forecasts do not begin the first rapid MSLP deepening until ~12 UTC 4 September (Figure 10c, blue and green dots). Both of these FCDI-based intensity forecasts rapidly decrease the MSLP approximately 7–8 mb in 6 h. It is noteworthy that the 15 min FCDI-based forecast then has a 7 h constant-intensity stage that matches the aircraft-observed timing and magnitude of the intermediate constant-intensity stage. By contrast, the hourly FCDI-based COAMPS-TC forecast continues the rapid MSLP deepening for the next 18 h very similar to the Control forecast. That is, the hourly FCDI-based COAMPS-TC forecast clearly misses the intermediate constant-intensity stage that the 15 min FCDI-based forecast captured very well. Furthermore, the 15 min FCDI-based forecast also resumed the rapid MSLP deepening at the correct time (03 UTC 5 September) according to the aircraft observations, and then had the correct deepening until the next set of aircraft observations approximately 9 h later centered on 12 UTC 5 September (Figure 10c, blue dots).

The ~10 mb deepening to 915 mb during 18 UTC 5 September to 00 UTC 6 September according to the NHC post-season best track was not predicted by the Control or either of the FCDI-based COAMPS-TC forecasts. Rather, all three of these COAMPS-TC forecasts predicted an essentially

constant intensity from 18 UTC 5 September until 18 UTC 6 September. The NHC best track also has a constant MSLP for the last 12 h, but at a pressure 15–20 mb lower than the three COAMPS-TC forecasts. The tentative hypothesis to be examined in the future is that these three COAMPS-TC forecast had an increasing poleward track forecast error (Figure 10b), and such a large poleward track error was not favorable for further deepening.

The 15 min FCDI-based COAMPS-TC z = 12,860 m vector wind forecast (Figure 11), which starts with the initial conditions of 18 UTC 3 September from Figure 6b, will be discussed first as the largest impacts of the AMVs are to be expected with that dataset. In just 24 h (Figure 11b), the outflow has greatly increased in areal extent and in magnitude, and especially in the northern semi-circle. A direct connection of the westward outflow branch with the short-wave trough in the northwest corner has resulted in an acceleration of the jet maximum in advance of that trough. The northward outflow branch has advanced poleward into a region where there was a ridge in the initial conditions (Figure 11a), and in conjunction with the northeastward outflow branch has deflected the previous northerly environmental flow to the east. Indeed, a northerly jet maximum is predicted near 19° N, 42° W in conjunction with these enhanced Irma outflow branches.

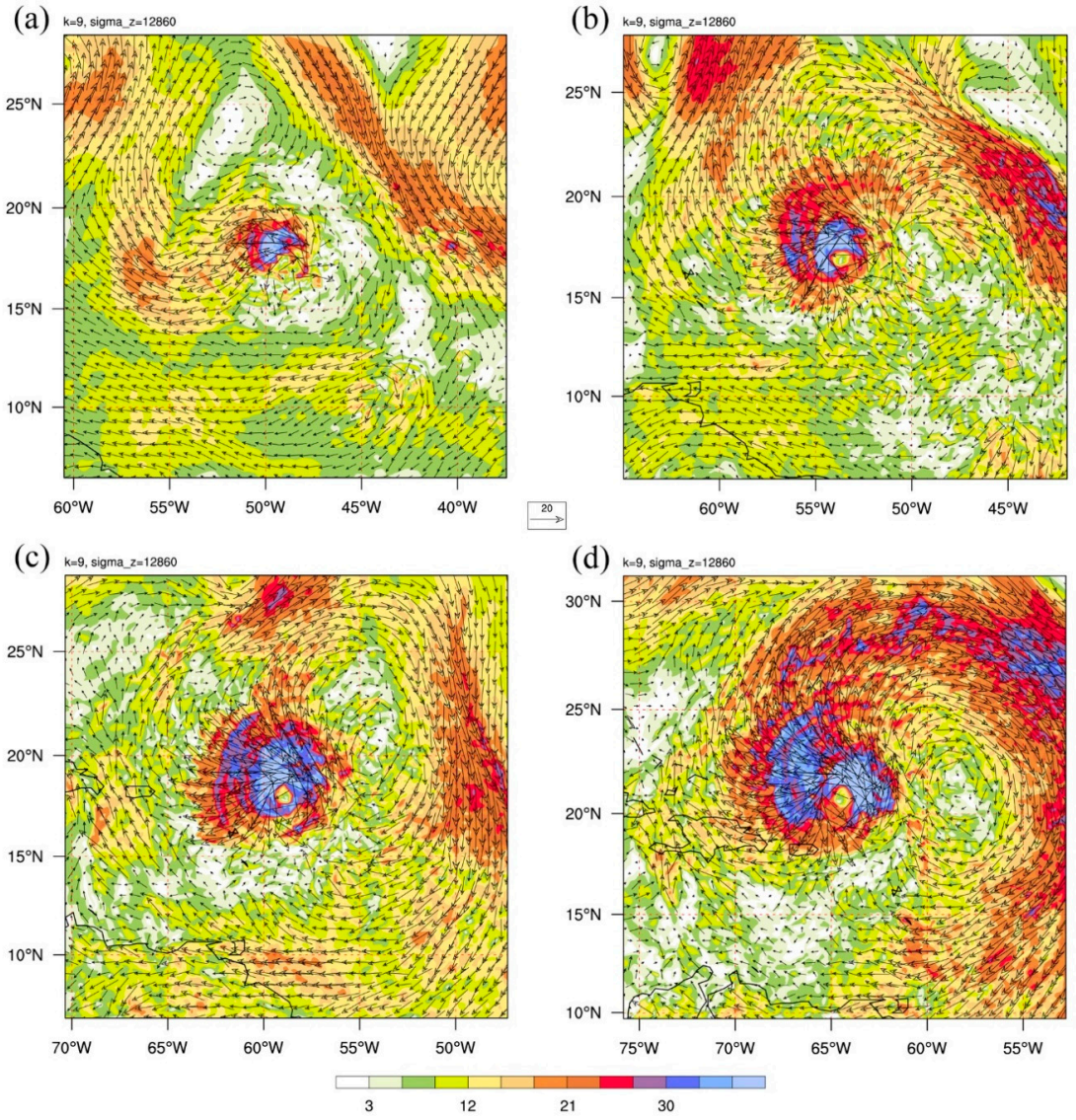

Figure 11. (**a**) Warm-start initial conditions (tau = 0 h) z = 12,860 m wind vectors (m s^{-1}; color bar and 20 m s^{-1} length indicated by arrow in middle) at 1800 UTC 3 September from the 15 min AMV FCDI analysis as in Figure 6d, and COAMPS-TC forecasts at (**b**) tau + 24 h, (**c**) tau + 48 h, and (**d**) tau + 72 h.

Between tau + 24 h in Figure 11b and tau + 48 h in Figure 11c the direct connection of the Irma outflow has weakened with the short-wave trough to the northwest that has now advanced to ~62° W, and has also weakened with the jet maximum to the east since there is an extensive region of light winds in the ridge to the northeast that is between the outflow and that jet to the east. These weakened connections of the Irma outflow with the adjacent synoptic systems may be associated with intermediate 12 h period of interrupted RI as documented by the aircraft observations in Figure 10c. However, another outflow burst is clearly in process at tau + 48 h (Figure 11c) compared to outflow areal extent and magnitude, especially to the west and to the north, relative to tau + 24 h (Figure 11b). Such a vigorous outflow is consistent with an ongoing RI of ~ 20 mb decrease from 18 UTC 4 September (tau + 24 h) to 18 UTC 5 September (tau + 48 h) in Figure 10c, although further study is required to quantify the timing of the outflow burst versus the RI timing. By tau + 72 h in Figure 11d, the outflow burst has continued and increased in magnitudes, and again especially to the west and to the northwest. Consequently, the direct connections of the Irma outflow with the adjacent synoptic circulations have been re-established as at tau + 24 h in Figure 11b. It is noteworthy that the outflow toward the northwest continues to have magnitudes > 30 m s^{-1} as it curves anticyclonically to connect with the jet maximum to the east. Rather than a weak anticyclone to the northeast of Irma as at tau + 48 h (Figure 11c), by tau + 72 h there is a large and intense anticyclone to the east that is trailing Irma. Such a strong outflow and connection to adjacent anticyclone is consistent with the intensity of ~935 mb for this 15 min FCDI-based COAMPS-TC forecast at 18 UTC 6 September (Figure 10c, blue dots).

Rather than a warm start from the six-hour COAMPS-TC forecast wind field at 18 UTC 3 September as in Figure 8a, the Control 72 h COAMPS-TC z = 12,860 m wind forecast begins from the cold-start COAMPS-TC initial conditions with a bogus vortex in Figures 8b and 12a. By tau + 24 h (Figure 12b), the outflow has increased to >30 m s^{-1} in the western semicircle, but there is not a direct connection to the short-wave trough and southerly jet to the northwest as in the 15 min FCDI-based COAMPS-TC forecast in Figure 11b. The outflow in the northeast quadrant is opposed by impinging northeasterly winds associated with the northerly jet farther to the northeast, which is very different from the strong outflow toward the northeast in Figure 11b. Recall from Figure 10c that the Control COAMPS-TC intensity forecast had two short (<6 h) intensifications followed by two constant-intensity (MSLP) periods within the first 24 h. It was only after tau + 22 h (16 UTC 4 September) that the Control forecast began a steady intensification, but during the first 12 h of that intensification was when the aircraft observations were indicating a constant intensity (MSLP).

The Control COAMPS-TC z = 12,860 m wind forecast at tau + 48 h (Figure 12c) has a ring of outflows around the center with magnitudes > 30 m s^{-1}. However, these outflows do not appear to be directly connected to the adjacent synoptic circulations. Rather, there is an outer ring of weak wind speeds, which suggests that there is a subsidence between the outflow and that outer ring. By tau + 72 h (Figure 11d), the Control forecast has strong outflow in the northern and the eastern quadrants that connects with the westerlies to the north and to a jet streak to the east and southeast, respectively. Whereas a strong ridge is trailing Irma in the 72 h Control COAMPS-TC forecast, the 15 min FCDI-based COAMPS-TC forecast has a large and intense anticyclone just to the east of Irma (Figure 11d). Nevertheless, both of these COAMPS-TC forecast have the same MSLP = 935 mb intensity at 18 UTC 6 September, which may be attributed to the Control forecast having begun the second RI segment too early according to the aircraft observations.

The 72 h COAMPS-TC z = 12,860 m wind forecast based on the initial conditions from the hourly AMV-based FCDI analysis at 18 UTC 3 September (Figure S1d) is presented in Figure 13. Because that initial analysis (repeated in Figure 13a) had strong outflow to the west of the center by tau + 24 h (Figure 13b) that outflow toward the west had strengthened and expanded in area and thus had a direct connection to the short wave trough and southerly jet to the northwest, which is quite similar to the 15 min AMV-based FCDI-based 24 h forecast in Figure 11d. Whereas there was northerly environmental flow impinging on the outflow in the northeast quadrant in the initial conditions,

by tau + 24 h (Figure 13b) the outflow in that quadrant was sufficiently strong to push away to the east the initial impinging environmental flow. However, the outflow toward the north and northeast in the 15 min FCDI-based COAMPS-TC forecast (Figure 11b) was even stronger and contributed to a strong ridge to the northeast with a direct connection to a jet streak to the east. In that aspect, the hourly FCDI-based forecast more resembles the Control forecast (Figure 12c), which had a region of light winds in the ridge to the northeast.

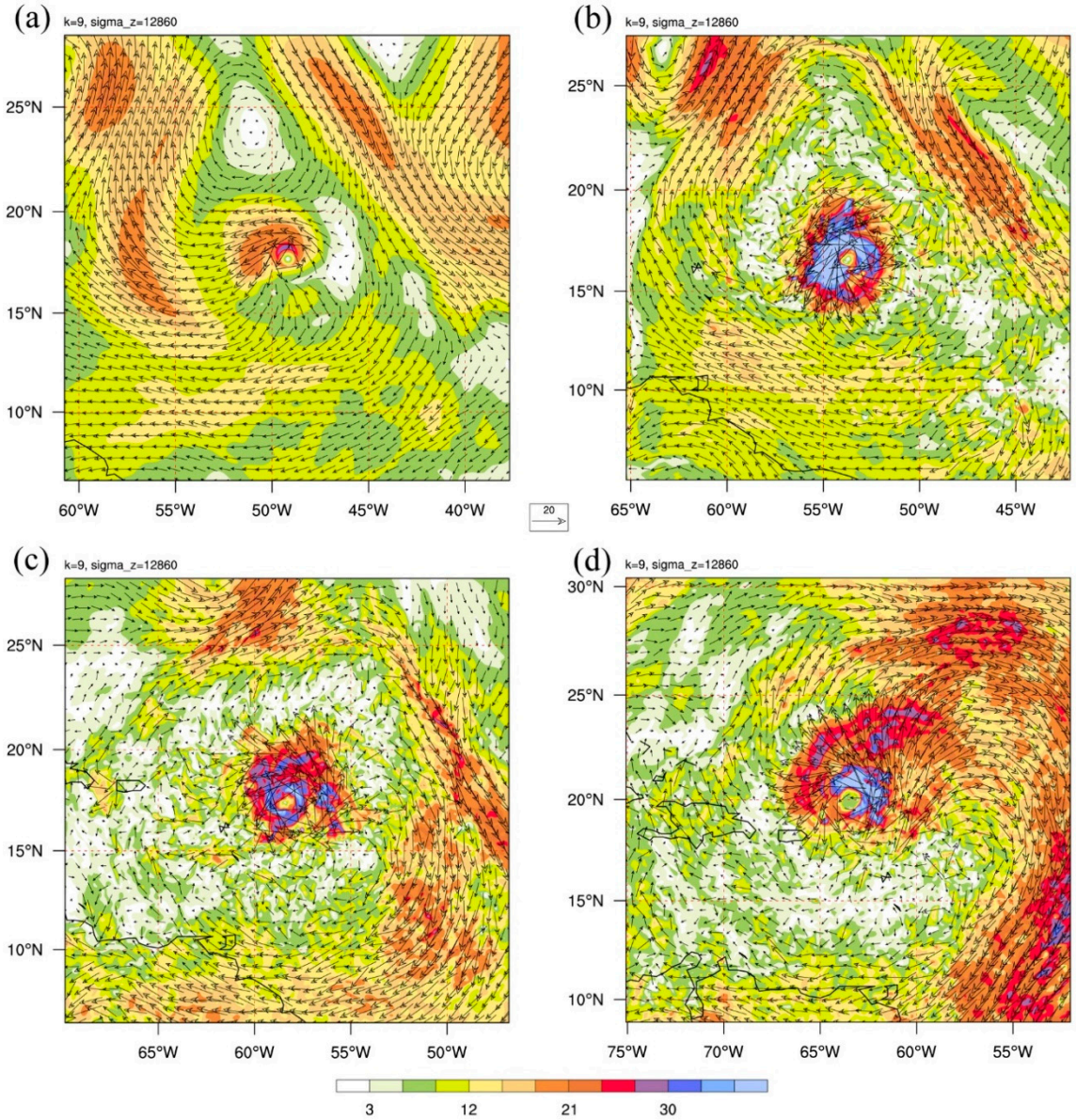

Figure 12. As in Figure 11, except from (**a**) cold-start COAMPS-TC initial conditions (tau = 0 h) at 1800 UTC 3 September as in Figure 8b, and then COAMPS-TC forecasts at (**b**) tau + 24 h, (**c**) tau + 48 h, and (**d**) tau + 72 h.

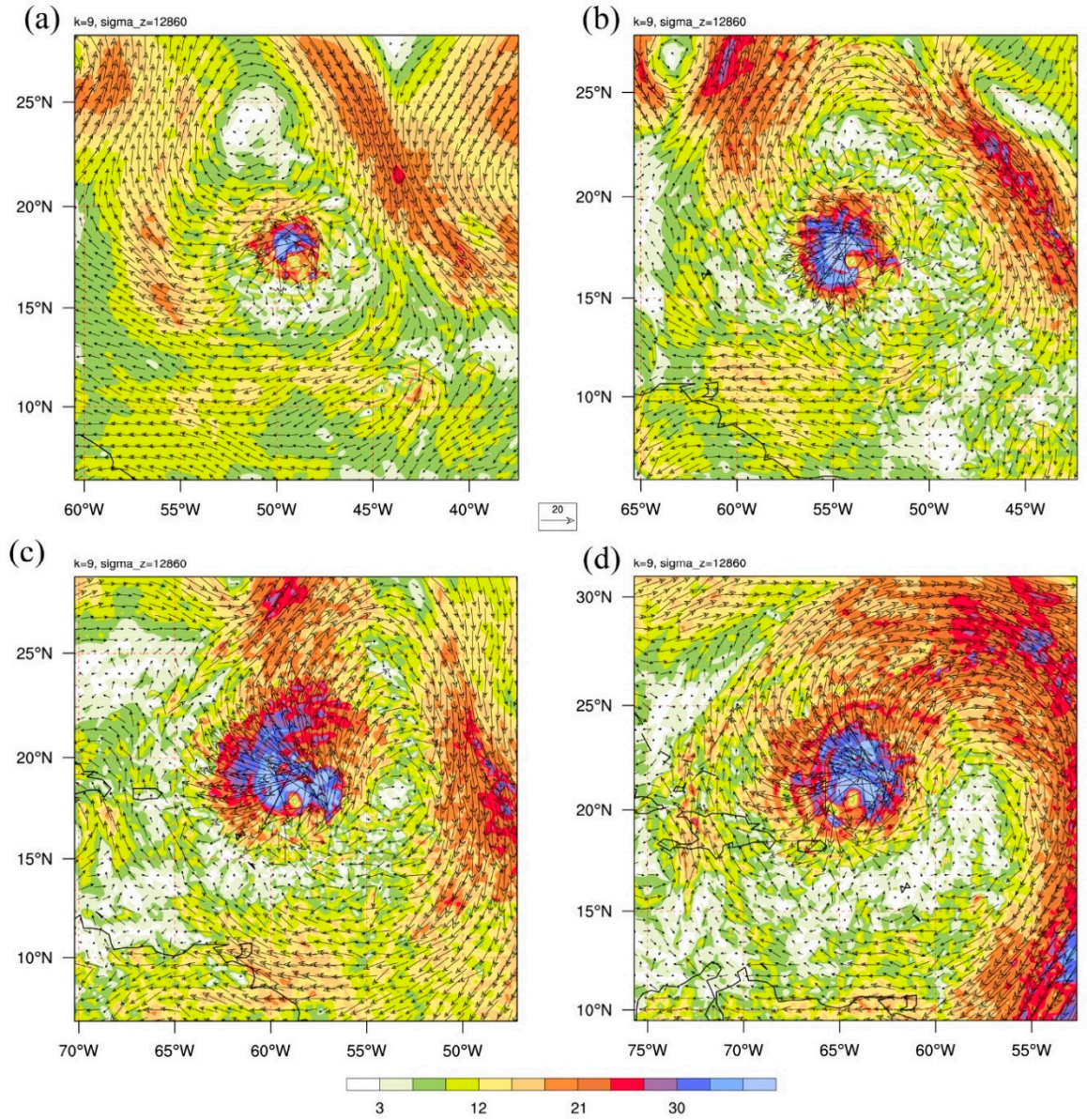

Figure 13. As in Figure 11, except from (**a**) warm-start initial conditions from the CIMSS hourly AMV FCDI analysis as in Figure S1 panel (d), and then COAMPS-TC forecasts at (**b**) tau + 24 h, (**c**) tau + 48 h, and (**d**) tau + 72 h.

Whereas the 15 min AMV FCDI-based COAMPS-TC tau + 48 h z = 12,860 m wind forecast (Figure 11c) had indications of a weaker interaction with adjacent synoptic circulations (possibly explaining the 12 h intermediate constant MSLP period), the hourly AMV FCDI-based forecast at tau + 48 h (Figure 13c) has a stronger outflow with a direct connection to the short wave trough and southerly jet to the north. This outflow distribution and strength may then explain why the hourly AMV FCDI-based intensity forecast (Figure 10c, green dots) continued the rapid intensification through the 12 h intermediate constant MSLP period according to the aircraft observations. By tau + 72 h (Figure 13d), the hourly AMV FCDI-based COAMPS-TC forecast of z = 12,860 m winds more closely resembles the 15 min AMV FCDI-based forecast (Figure 11d) than it does the Control COAMPS-TC forecast (Figure 12d). Whereas the hourly AMV FCDI-based forecast has a single outflow dome oriented toward the north, the 15 min AMV FCDI-based forecast has a stronger outflow dome oriented toward the west plus a second outflow dome in the northeast quadrant. Nevertheless, the 72 h intensity forecast for the hourly

AMVs has a slightly deeper MSLP (Figure 10c, green dots), which may be attributed to its continued RI without predicting the 12 h intermediate constant MSLP period as in the aircraft observations.

The COAMPS-TC z = 300 m vector wind forecasts corresponding to the z = 12,850 m vector wind forecasts in Figures 11–13 are difficult to intercompare because the differences are concentrated within ± 200 km of the centers. Consequently, isotach analyses at z = 300 m in Figure S3b for the 15 min AMV FCDI-based analysis, and in Figure S3d for the hourly AMV FCDI analysis, will be the format for the COAMPS-TC z = 300 m forecast comparisons.

In the warm-start initial conditions for the 15 min AMV FCDI-based COAMPS-TC forecast (Figure 14a), one small 55 m s^{-1} isotach maximum is just to the east of the center and the second small 55 m s^{-1} isotach is to the southwest of the center. At tau + 24 h (Figure 14b), the isotach maximum exceeds 65 m s^{-1} and the inner isotachs are elliptical in shape with a north-south major axis. The RMW to the north is ~ 55 km. At tau + 48 h (Figure 14c), an elliptical ring of isotachs > 65 m s^{-1} encompasses the center, and the major axis is oriented northwest-southeast. There is some indication of a secondary 60 m s^{-1} isotach maximum in the northeast quadrant at a radius ≈ 70 km. By tau + 72 h (Figure 14d), the isotachs near the center are more circular rather than elliptical as in Figure 14b,c, and they are U-shaped rather than having a linear decrease to zero at the center.

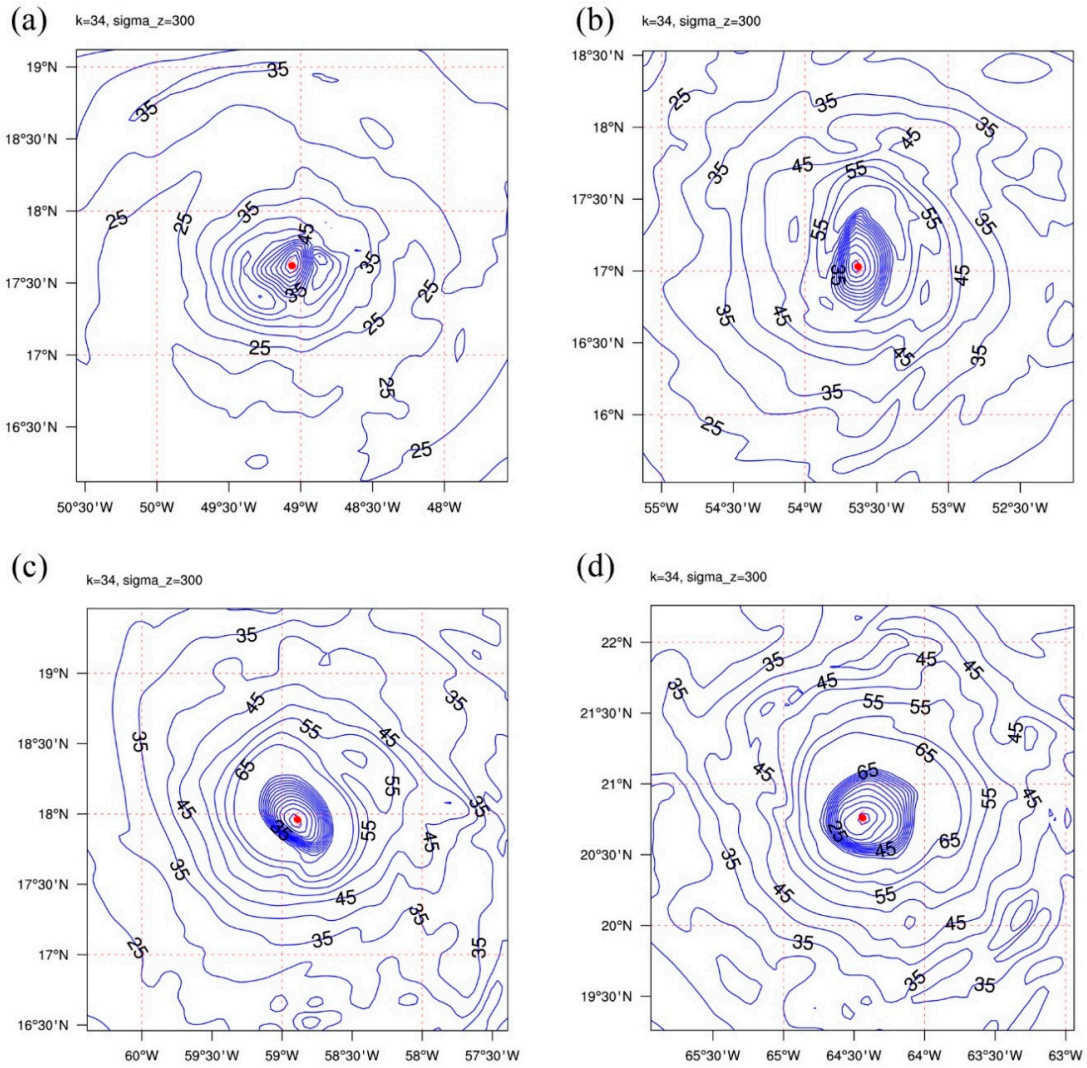

Figure 14. (**a**) Warm-start initial conditions (tau = 0 h) at 1800 UTC 3 September from the 15 min AMV FCDI analysis, and then COAMPS-TC forecasts at (**b**) tau + 24 h, (**c**) tau + 48 h, and (**d**) tau + 72 h for z = 300 m wind isotachs at 5 m s^{-1} intervals from 5 to 65 m s^{-1}.

The Control COAMPS-TC z = 300 m isotach forecast begins at 18 UTC 3 September as a cold start with a bogus vortex that is superposed on a background steering flow such that the $V_{max} \approx 55$ m s^{-1} is at RMW ≈ 37 km to the north of the center (Figure 15a). Recall from Figure 10c (gold dots) that this Control forecast began with a MSLP ≈ 960 mb and had two very rapid (<6 h) deepening periods within the first 12 h and then maintained a near-constant MSLP for ≈ 8 h. In terms of the COAMPS-TC z = 300 m isotach forecast at tau + 24 h (Figure 15b), a broad nearly symmetric ring of wind speeds exceeding the largest (65 m s^{-1}) isotach displayed is predicted, with increases as large as 30 m s^{-1} at 35 km and beyond to the south of the center. Furthermore, the isotachs near the center are U-shaped rather the linear decrease from the RMW to the center, which is another indication of a very intense storm. By tau + 48 h (Figure 15c), the ring of wind speeds exceeding 65 m s^{-1} has contracted, and the Control forecast has already reached a MSLP ≈ 925 mb (Figure 10c) by tau + 42 h (12 UTC 5 September). By tau + 72 h (Figure 15c), a slight weakening is suggested by the less broad ring of >65 m s^{-1} winds, a linear decrease in speed is predicted from the RMW to the center, and a highly elliptical isotach pattern exists near the center (resembling the tau + 48 h pattern in Figure 14c).

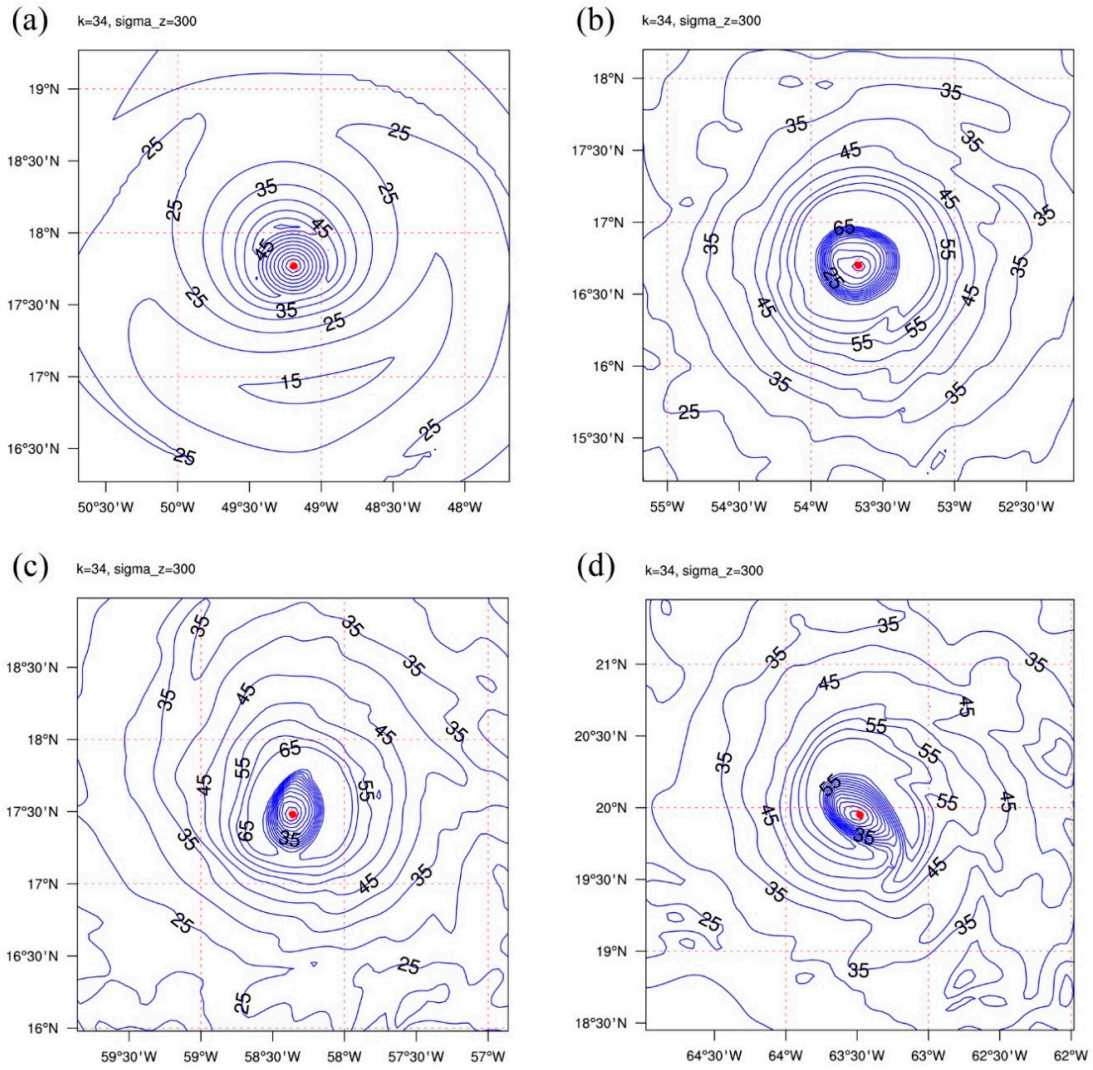

Figure 15. As in Figure 14, except from (**a**) the cold-start COAMPS-TC initial conditions (tau = 0 h) at 1800 UTC 3 September as indicated in Figure 8b, the COAMPS-TC forecasts at (**b**) tau + 24 h, (**c**) tau + 48 h, and (**d**) tau + 72 h.

Now consider the hourly GOES-13 AMV FCDI-based COAMPS-TC z = 300 m isotach forecast (Figure 16) in comparison with 15 min GOES-16 AMV FCDI-based (Figure 14) and Control (Figure 15)

COAMPS-TC forecast. As described above in the discussion of Figure S3d, the hourly FCDI-based z = 300 m initial conditions in Figure 16a resemble the 15 min FCDI-based initial conditions in Figure 14a with slightly weaker inner-core wind vectors. Thus, the hourly FCDI-based tau + 24 h z = 300 m isotach forecast (Figure S3b) also resembles the 15 min FCDI-based tau + 24 h forecast, except that the maximum wind speeds > 65 m s^{-1} are in the western semicircle rather than in the northern semicircle. By contrast, the Control isotach forecast has predicted an asymmetric ring of maximum wind speeds >65 m s^{-1} at tau + 24 h (Figure 15b). Again at tau + 48 h (Figure 16c) the hourly FCDI-based forecast has the same isotach pattern as the 15 min FCDI-based forecast (Figure 14c), but the tight isotach spacing indicates a more intense vortex (lower MSLP) as the hourly FCDI-based forecast continues to deepen through the 12 h intermediate constant-intensity period that was documented by aircraft observations (Figure 10c, green dots). At tau + 72 h (Figure 16d), the hourly FCDI-based forecast isotach pattern more resembles the Control isotach pattern (Figure 15d) with an elliptical shape and northwest-southeast major axis. Thus, it is encouraging that the hourly GOES-13 AMV dataset as in Figure 1 can provide initial conditions for a rapid intensification of Irma as predicted by the Control forecast. However, both the hourly FCDI-based and the Control COAMPS-TC did not predict (or missed the timing) of the 12 h intermediate constant MSLP period that is a unique characteristic of the Irma RI, and the 15 min FCDI-based COAMPS-TC forecast did predict that characteristic.

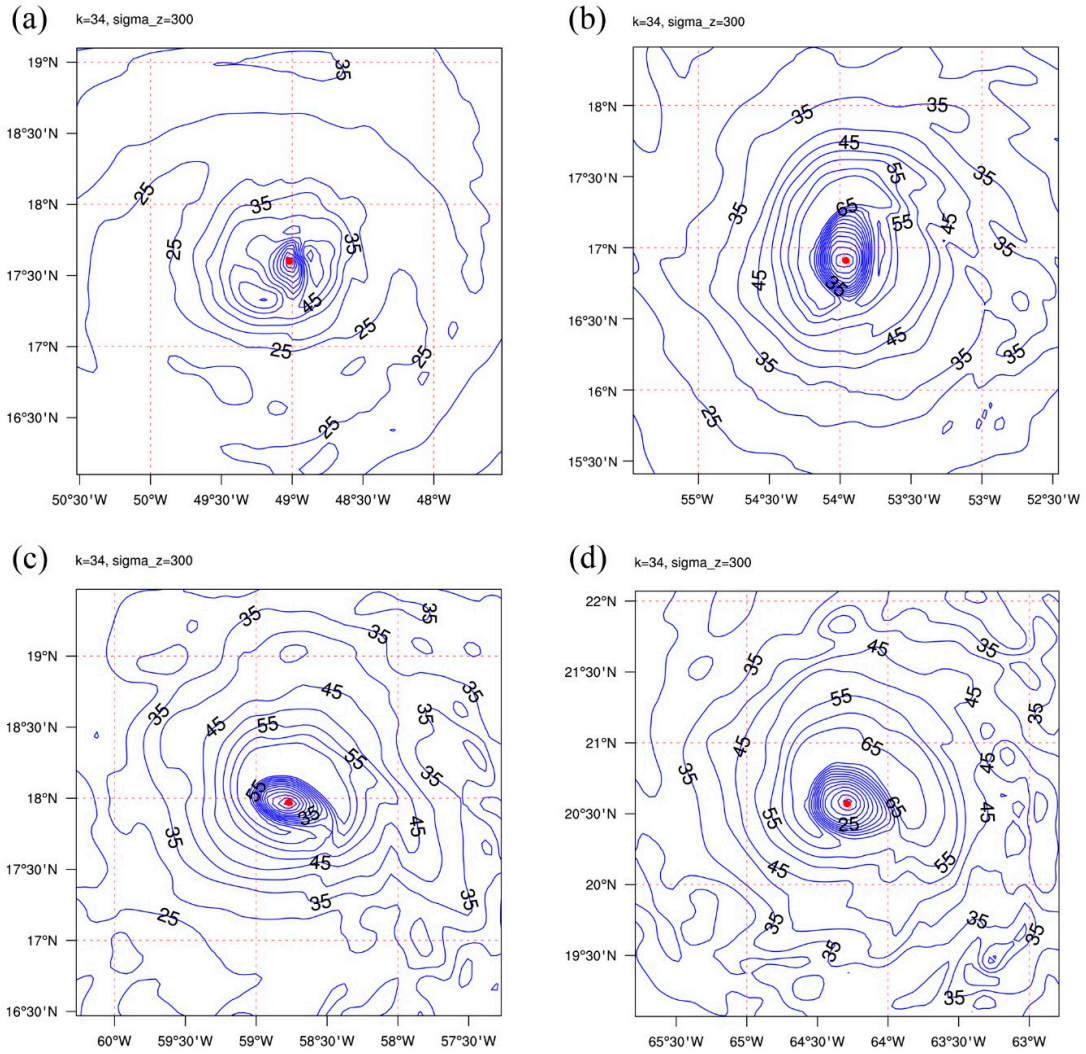

Figure 16. As in Figure 14, except from (**a**) the initial conditions from the CIMSS hourly AMV FCDI analysis at 1800 UTC 3 September as indicated in Figure S1d, and then COAMPS-TC forecasts at (**b**) tau + 24 h, (**c**) tau + 48 h, and (**d**) tau + 72 h.

3. Comparison with HWRF Initialization and Forecasts

Lewis et al. (2020) [6] explored different strategies for assimilating the same high-density AMV dataset in Hurricane Irma (2017) that has been utilized here in the FCDI analysis. Lewis et al. [6] utilized the 2019 version of the NCEP HWRF model to document the impacts of observation pre-processing and also evaluated AMV thinning and adjustments to observation errors. They documented that the high-density vortex-scale GOES-16 AMVs in Figure 1b led to notable decreases in the HWRF track forecast errors over the Irma lifecycle compared to the Control experiment without the high-density AMVs. However, the impacts on the Irma intensity and structure (i.e., wind radii) forecast errors were less robust [6].

In this section, the Lewis et al. [6] HWRF initialization at 18 UTC 3 September and subsequent 72 h HWRF model forecast of the Irma RI event will be compared with the 15 min GOES-16 AMV FCDI analysis and 72 h COAMPS forecast. Since different models are being utilized, the HWRF initialization and model forecast with the high-density GOES-16 AMVs will also be compared to a Control HWRF without the high-density AMVs. These HWRF datasets were kindly provided by William E. Lewis in response to our request.

The comparison of the Control and high-density AMV-based HWRF 72 h track forecasts with the NHC best track in Figure 17a is very similar to the Control and 15 min AMV FCDI-based COAMPS-TC track forecasts in Figure 10c. That is, both HWRF track forecasts are highly accurate during the southward-drift segment of the Irma track, but then both track forecasts have too large poleward deviations with the high-density AMV along-track forecast being faster than for the Control. The same track forecast error tendencies were found for the COAMPS-TC forecasts in Figure 10b. Thus, for this specific 18 UTC 3 September track forecast initiated prior to the Irma RI event, the GOES-16 AMVs did not have a favorable impact for either the HWRF or the COAMPS-TC track forecast.

Due to the sophisticated HWRF vortex initialization procedure, the Lewis et al. [6] tau = 0 h MSLP for both the Control and the high-density AMV HWRF intensity forecasts is equal to the NHC best-track value at the initial time of 18 UTC 3 September (Figure 17b). However, both HWRF model forecasts rapidly deepen the MSLP by 15 mb in 12 h and more than 25 mb in 24 h. As was the case for the Control COAMPS-TC MSLP forecast in Figure 10c, the Control HWRF forecast (Figure 17b, blue line) has an earlier 12 h period of constant MSLPs before the intermediate constant MSLP period in the NHC best track that is based on aircraft observations (Figure 17b, black line). Indeed, the Control HWRF forecast has an 8 mb deepening during that 12 h constant MSLP period, and continues to rapidly deepen Irma until tau + 72 h with a MSLP of 908 mb, which is an overdeepening by 10 mb.

Whereas the 15 min AMV FCDI-based COAMPS-TC forecast has accurately predicted the timing and duration of the 12 h intermediate constant MSLP period (Figure 10c, blue dots), the HWRF forecast from an initialization that included those high-density AMVs continued that rapid deepening right through that constant MSLP period that is based on aircraft in situ observations (Figure 17b, red line). Although the HWRF had a perfect MSLP forecast at tau + 48 h, this must be considered a coincidence given the overdeepening between tau = 0 h and tau + 12 h and tau + 24 h, and then completely missing the constant MSLP period. The Control HWRF forecast at least did predict a 12 h constant MSLP period that was 12 h premature. Thus, the addition of the high-density AMVs not only did not correct that incorrect timing, they contributed to elimination of that 12 h constant MSLP period due to the HWRF prediction of a continuous rapid deepening.

Thus, the question is why/how did the GOES-16 AMVs contribute to the FCDI analysis that led to a more accurate COAMPS-TC forecast than the Control COAMPS-TC forecasts (Figure 10c), but did not similarly contribute to a more accurate high-density AMV HWRF MSLP forecast (Figure 17b, red line). Some key components in the HWRF initialization procedure were compared with the FCDI analysis procedure in Sections 2.1.2 and 2.1.3. The HWRF initial conditions for z = 12,860 m at 18 UTC 3 September (Figure 18a) for the Control HWRF forecast has a similar depiction of the adjacent synoptic features as in the Control COAMPS-TC initial conditions in Figure 12a. However, the HWRF initialization has much stronger (>30 m s^{-1}) outflow vectors in a more concentrated area

than the ≈21 m s^{-1} outflow vectors near the center in the Control COAMPS-TC initial conditions. One key difference is the HWRF outflow toward the northeast is so strong that the outflow has pushed back the impinging northerly environmental flow that is encroaching on the outflow in the Control COAMPS-TC initial conditions. Consequently, there is a continuous band of light winds between the outflow and the northerly environmental flow to the northeast in the Control HWRF initial conditions, which should favor a more rapid deepening.

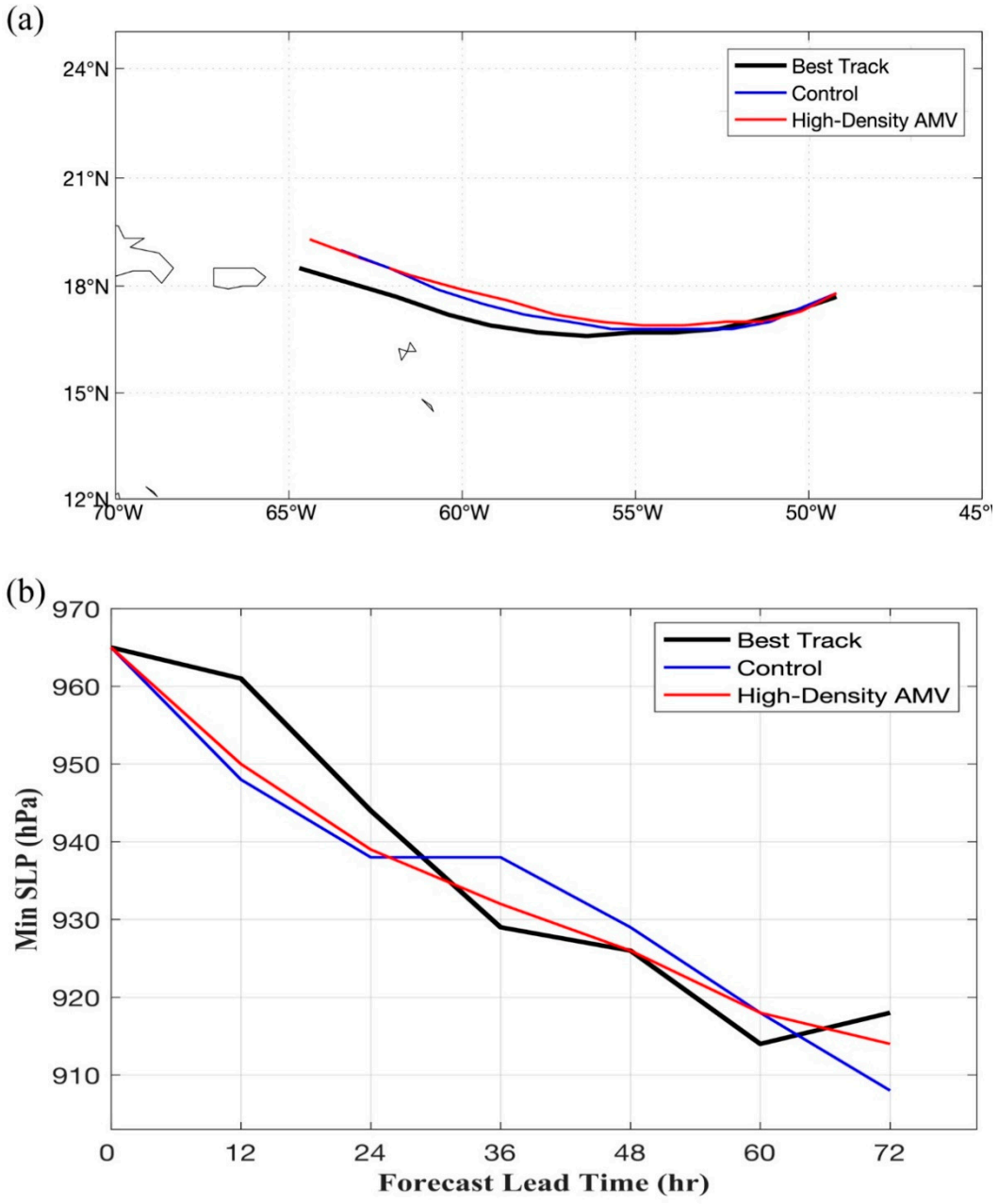

Figure 17. (**a**) Irma best track (black line) between 18 UTC 3 September and 18 UTC 6 September as in Figure 10b compared with CIMSS Control HWRF track forecast (blue line) and high-density AMV HWRF track forecast (red line). (**b**) As in panel (**a**), except for MSLP (hPa) instead of track (provided by William E. Lewis, CIMSS).

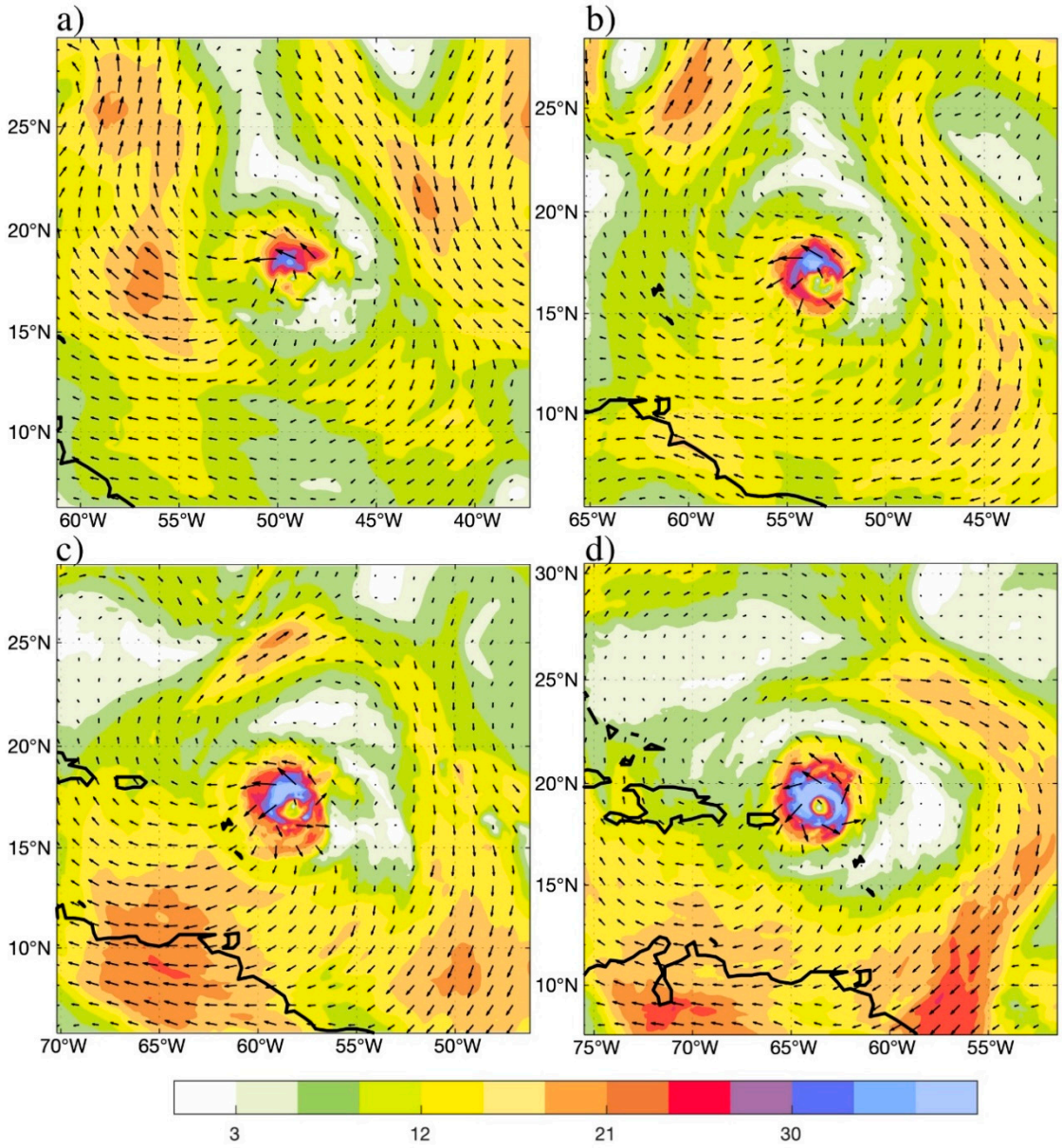

Figure 18. As in Figure 12, except for the Control HWRF without the high-density AMV datasets. (**a**) Initialization for z = 12,860 m wind vectors (m s^{-1}, color bar at bottom) at 18 UTC 3 September, and then the HWRF model forecasts at (**b**) tau + 24 h, (**c**) tau + 48 h, and (**d**) tau + 72 h (provided by William E. Lewis, CIMSS).

By tau + 24 h (Figure 18b), the HWRF forecast outflow is slightly stronger to the north of the center, but has a minimum outflow in a comparable size area to the south. Similar to the Control COAMPS-TC forecast at tau + 24 h (Figure 12b), the outflow toward the west is diminished and consequently the direct connection to the short wave trough and southerly jet maximum to the northeast is markedly reduced compared to the initial conditions in Figure 18a. It is noted that the reduction in the direct connection is much clearer in the Control COAMPS-TC forecast because a broad region of light winds is predicted between the strong outflow toward the west and the entrance to the southerly jet farther to the west (Figure 12b). Whereas the region of light winds between the outflow and the northerly environmental flow to the northeast of Irma simply continued in the Control HWRF, a wider region of light winds (Figure 12b) had replaced the impinging northerly environmental flow that had existed in the Control COAMPS-TC at the initial time (Figure 12a). It is proposed that these changes in the outflow pattern and magnitude, and in the direct connections with the adjacent synoptic circulations,

are consistent with an early intermediate period of constant MSLP between tau + 24 h and tau + 36 h in the Control HWRF (Figure 17b) versus between tau + 12 h and tau + 18 h in the Control COAMPS-TC (Figure 10c, gold dots). Future analysis of the forecast wind fields prior to and during these intermediate forecast intervals is necessary to determine whether the same physical processes in the HWRF model and in the COAMPS-TC model may have contributed to the intermediate constant MSLP periods in the two models.

By tau + 48 h in the Control HWRF forecast (Figure 18c), the same pattern of outflow vectors near the center existed as in the tau + 24 h forecast (Figure 18b), but with a small (<6 m s^{-1}) increase in magnitude. The major change has been an enhanced direct connection with an easterly jet region with a maximum near 9° N, 65° W that had increased in speed from >12 to >24 m s^{-1} in 24 h. There has also been an increase in speed of a northerly jet maximum centered near 8° N, 49° W, but that jet enhancement does not appear to be related to the Irma outflow. Thus, the interpretation is that the extremely rapid intensification in the Control HWRF forecast from tau = 0 to tau + 24 h (Figure 17b) had sent an outflow pulse to the south-southwest that had initiated an easterly speed maximum by tau + 24 h (Figure 18b). Even though the MSLP was constant from the tau + 24 h to tau + 36 h (Figure 17b), the outflow pulse to the south had continued and was enhanced by 48 h such that strong easterly jet was generated. It is likely that the far southward penetration of the outflow pulse was associated with the small Coriolis parameter being less effective in anticyclonically turning the flow to the west.

As the Control HWRF forecast continued the rapid deepening of Irma from 938 mb at tau + 36 h to 908 mb at tau + 72 h (Figure 17b), a ring of strong (>36 m s^{-1}) outflow then enclosed the center (Figure 18d). However, an almost complete ring of small vectors is predicted at larger radii that then confines the outflow and mostly prevents a connection to adjacent synoptic circulations. Presumably the outflow subsides within this region of small vectors, and Irma in the HWRF forecast is an isolated intense vortex at z = 12,860 m with a center that is directly over the z = 250 m center (see Figure S4d).

The high-density AMV HWRF initial conditions for the z = 12,860 m wind vectors (Figure 19a) are very similar to the Control HWRF (Figure 18a) beyond 300 km radius. The outflow magnitudes are slightly smaller near the center than in the Control HWRF, except the outflow is stronger to the west, which was also the case for the 15 min AMV FCDI-based COAMPS-TC initial conditions (Figure 11a). Both of these high-density AMV HWRF and COAMPS-TC initial conditions have a broad semicircle of light winds on the eastern side that prevents the northerly environmental flow farther to the east from interacting with the outflow.

By tau + 24 h (Figure 19b), the high-density AMV HWRF forecast has slightly stronger outflow in the northwestern semicircle than in the Control HWRF (Figure 18b), and the outflow pulse is stronger and more directed toward the southwest than toward the south in the Control. These differences in the outflow pulse to the southwest appear to be the only explanation for why the high-density AMV HWRF forecast continued to rapidly deepen (Figure 17b, red line) through the 24–36 h forecast interval while the Control HWRF forecast had constant MSLP. An extensive band of light winds to the northeast of the center is predicted in both HWRF forecasts, which restricts the outflow in that direction, and there is no direct connection with the jet maximum in the northerly environmental flow farther to the east.

The contrast of this high-density AMV HWRF tau + 24 h forecast of the z = 12,860 m winds with the corresponding 15 min AMV FCDI-based COAMPS-TC tau + 24 h forecast (Figure 11b) is very striking. The COAMPS-TC forecast has much stronger outflow in all directions that then extend to larger radii. The outflow toward the west leads to a more direct connection to the short wave trough to the west with an associated enhancement of the southerly jet to the east of that trough. The outflow to the north and the northeast in the COAMPS-TC forecast have crossed the light wind region to the northwest of the center in the HWRF forecast and thus has a direct connection with a >30 m s^{-1} jet maximum in the northerly environmental flow. As indicated above, no such connection exists in the HWRF tau + 24 h forecast as the outflow to the northeast is confined to within ≈200 km.

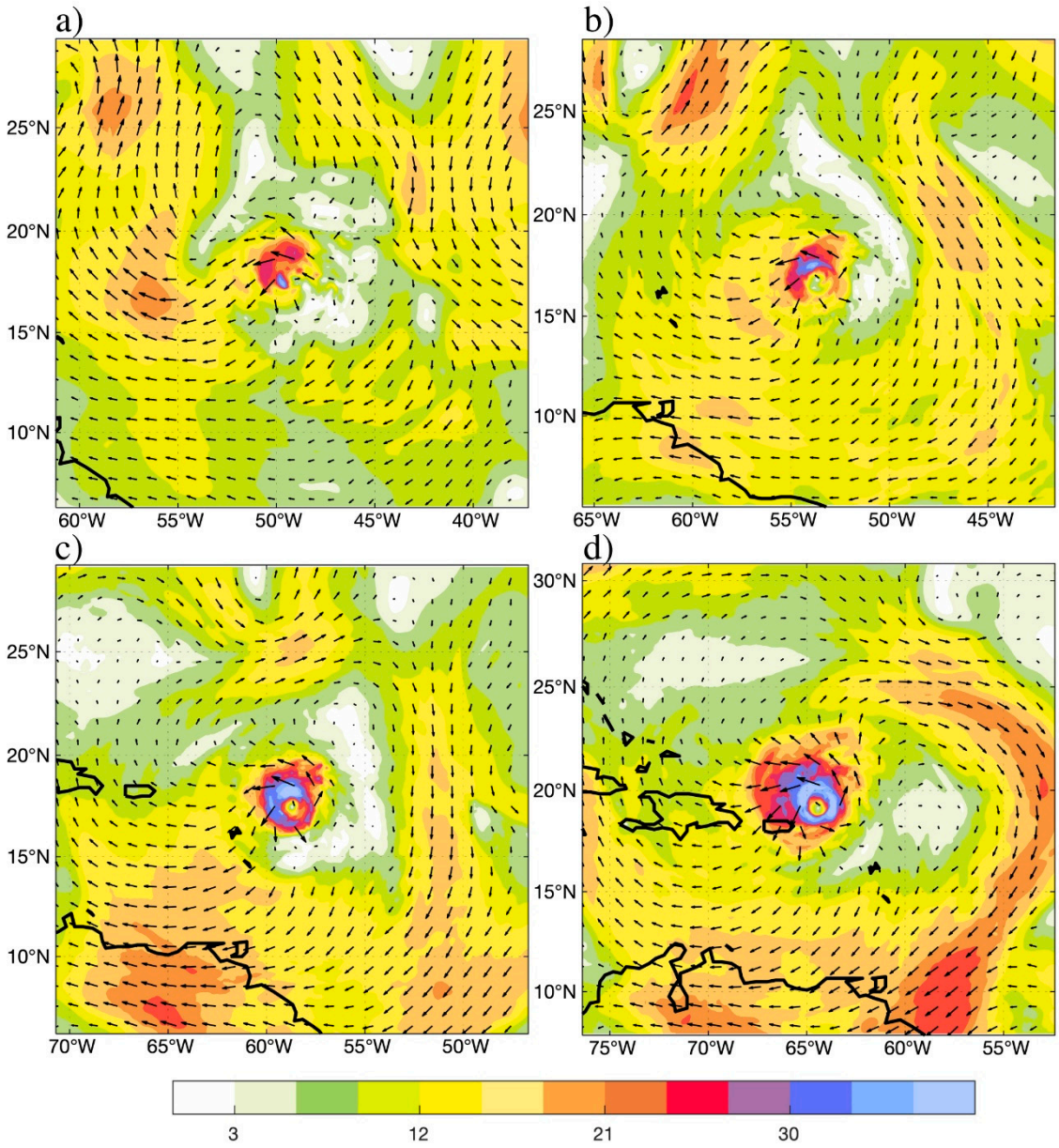

Figure 19. As in Figure 18, except z = 12,860 m wind vectors for the HWRF model forecast with (**a**) the CIMSS high-density AMV dataset included in the HWRF vortex initialization at 18 UTC 3 September, and then the HWRF model forecasts at (**b**) tau + 24 h, (**c**) tau + 48 h, and (**d**) tau +72 h. (provided by William E. Lewis, CIMSS).

At tau + 48 h (Figure 19c), the high-density AMV HWRF forecast is almost identical to the Control HWRF forecast (Figure 18c), both in terms of the outflow pattern and the magnitudes near the center. Both of these HWRF forecasts were rapidly deepening the Irma vortex at approximately the same rate from tau + 48 h to tau + 72 h (Figure 17b). However, the 72 h high-density AMV HWRF forecast of the outflow magnitude and connection to adjacent synoptic features (Figure 19d) is quite different from the Control HWRF forecast (Figure 18d), which had an isolated vortex outflow with a small connection to the jet region to the southwest. That is, the high-density AMV HWRF forecast had a ring of >36 m s^{-1} outflow vectors around the center, and a northward outflow direct connection to the jet streak to the east. Although this stronger outflow connected to the jet streak to the east, and predicted an anticyclone between Irma and the jet streak that is similar to the flow pattern at z = 12,860 m in the

15 min AMV FCDI-based COAMPS-TC forecast (Figure 11d), the high-density AMV HWRF forecast features at 72 h are considerably weaker.

The corresponding z = 250 mb wind forecasts by the Control HWRF and by the high-density AMV HWRF are in Figures S4 and S5, respectively. Because these wind forecasts are plots in the same format as the z = 12,860 m HWRF wind forecasts in Figures 18 and 19, it is difficult to quantify differences within the 20 m s^{-1} isotach. A key feature in the HWRF forecast is that the HWRF initialization at 18 UTC 3 September (Figure S4a) indicates a symmetric, compact vortex with a ring of wind speeds exceeding the 65 m s^{-1} maximum isotach in this plot, when at this time the NHC best-track intensity was 100 kt [5] (and in the working best track in real time). That is, although the HWRF initialization has matched the 965 mb best track (Figure 17), the corresponding maximum wind speed at 250 m is much higher (>65 m s^{-1}) than would be expected with a 100 kt (≈50 m s^{-1}) surface wind speed. By tau + 24 h (Figure S4b), the 20 m s^{-1} isotach is slightly increased in diameter, and the width of the ring of wind speeds exceeding 65 m s^{-1} is also wider, which implies a further increase in V_{max}. Both of these horizontal wind structure characteristics are increased in the Control HWRF forecast at tau + 48 h (Figure S4c), and again at tau + 72 h (Figure S4d). Thus, the Control HWRF forecast begins from a compact intense vortex and steadily increases the intensity and slightly broadens the size of the inner vortex over a 72 h period.

The surprising aspect of the high-density AMV HWRF initialization of the z = 250 m wind field (Figure S5a) is how small the differences are from the Control HWRF initialization (Figure S4a). A small weakening of the intensity is indicated by the smaller ring of wind speeds exceeding 65 m s^{-1} and a slightly larger diameter of 20 m s^{-1} isotach. However, the high-density AMV HWRF forecast at tau + 24 h (Figure S5b) is almost identical to the Control HWRF forecast at that time. By tau + 48 h (Figure S5c), the high-density AMV HWRF forecast has a slightly larger diameter 20 m s^{-1} isotach, but inner-core appears to be identical to the Control HWRF forecast. Except for a small tau + 72 h position difference, the high-density AMV HWRF forecast of the z = 250 m wind field is essentially identical to the Control HWRF forecast. Thus, the high-density AMVs have a minimal effect on the HWRF initialization of Hurricane Irma at 18 UTC 3 September, and that effect does not have a substantial effect on the z = 250 m horizontal wind structure HWRF forecast.

4. Summary and Concluding Remarks

4.1. Summary

This study has explored the opportunities for improved wind field analyses and numerical model initial conditions utilizing high spatial and temporal (15 min) resolution atmospheric motion vectors (AMVs) such as Figure 1b now available from the new-generation geostationary meteorological satellite GOES-16. The CIMSS special processing strategies greatly enhanced the AMV coverage to resolve the small scales of the flow fields associated with the Irma vortex and its near environment [6]. In addition to the routine GOES-16 full-disk scan every 10 min and the Continental U.S. scanning every 5 min, the meso scan mode with one-minute image sampling is moveable and targeted the Hurricane Irma center within a 10° latitude by 10° longitude domain [7]. Using this one-minute imagery, CIMSS has developed automated algorithms to produce these enhanced high spatial resolution AMVs. Most importantly, the one-minute imagery can detect the inner-core outflow AMVs at elevations above 150 mb (Figure 1b, red vectors) that define the "outflow dome" that is highly asymmetric. Comparisons of vortex-scale wind analyses with these AMVs have been made with the COAMPS-TC model analyses and forecasts as a Control, and with analyses produced from only the lower-density hourly AMVs from GOES-13 (Figure 1a).

Feng and Wang (2019) [16] have investigated the impact of the NASA WB-57 dropwinsondes deployed from 60,000 feet over Hurricane Patricia (2015) during its RI phase. These High-Density Sounding System (HDSS) sondes were deployed as frequently as every 4 km during overpasses of the center and measured zonal and meridional wind components, temperature, and moisture.

Therefore, the unique time scales of the near-storm outflow and the inner-core vortex structure aloft could be resolved. Feng and Wang [16] used an ensemble-variational data assimilation system in which the HDSS observations were superobbed within a spatial grid box of 4 km × 4 km in the horizontal and within 10, 50, and 20 hPa layers at lower, middle, and upper levels, respectively, to better resolve the fine spatial and temporal structure with the data assimilation system. The accuracy of the near-storm outflow analyses were verified in this Patricia case against a special CIMSS re-processed GOES-13 AMV dataset analogous to the GOES-13 AMV dataset for Hurricane Joaquin (2015) utilized by Elsberry et al. [1,3] and Hendricks et al. [2]. If the GOES-13 AMV dataset used by Feng and Wang [16] had limited coverage over the inner core as in Figure 1a, then the outflow dome at elevations above 150 mb over Patricia would not have been resolved, and this may be the reason that the Feng and Wang [16] outflow verification was only in the "near-storm" region. It is highly likely that the HDSS sondes deployed from 60,000 feet at ~4 km horizontal spacing during center overpasses would have provided high resolution vertical cross-sections through the Patricia outflow dome. Unfortunately, no NASA WB-57 missions with HDSS sondes exists over Hurricane Irma (2017) that could have been used to verify the FCDI outflow dome analyses in this study.

The challenge has been to assimilate the extremely high-density GOES-16 AMVs every 15 min for six hours without data thinning that other groups such as Lewis et al. [6] and Sawada et al. [12] have explored. Elsberry et al. [1] had utilized a dynamic initialization technique to incorporate into the COAMPS-TC and the NAVGEM a special GOES-13 dataset of 15 min AMVs reprocessed by the CIMSS during the lifecycle of Hurricane Joaquin (2015). Four modifications of the Elsberry et al. [1] technique were necessary for studying the RI in Irma, which was a challenging event that began on 4 September and continued to midday on 5 September, by which time Irma had strengthened from 100 kt to a category-5 hurricane with maximum sustained winds of 155 kt [5]. Based on both the SATCON and the NHC WBT intensity changes, four periods of the Irma RI are defined that are well supported by aircraft MSLP observations: (i) the pre-extreme RI period; (ii) the extreme RI period; (iii) the intermediate constant-intensity period; and (iv) the extended slower RI period.

The first modification of the Elsberry et al. [1] technique was to calculate the AMV-based wind increments with the FCDI dynamic initialization in which the raw AMV zonal and meridional wind components are inserted into the COAMPS-TC model for direct calculation of the nudging term. This has been shown to be a straight-forward and efficient technique for assimilating in near-real time the high temporal and spatial resolution GOES-16 AMVs reprocessed by CIMSS [7] without any thinning. The second modification has been to expand the sizes of Domains 2 and 3 to encompass the areas of the high temporal (15 min) GOES-16 AMVs, and also to apply the FCDI technique in the oceanic areas of Domain 1 utilizing the lower density hourly AMVs, which had not been done in Elsberry et al. [1]. The third modification has been to add a surface wind field adjustment in which a 300 km by 300 km and 1500 m deep layer centered on the Irma position is used as a constraint on the regions of deep convection relative to the center, which then facilitates a connection between the boundary layer ascent with the cloud-top divergence inferred from the AMVs. Another objective of the continued adjustment of the surface wind field to move along the target pathway toward the known 6 h ending position has been to ensure that the analyzed 6 h position is sufficiently close to the next warning position that the next assimilation cycle target position may then begin from the previous assimilation 6 h position with no vortex relocation or introduction of a bogus vortex being necessary. The Elsberry et al. [1] unique upscaling of the AMV-enhanced Domain 2 analysis to the NAVGEM to replace its synthetic vortex, and thereby improve its TC track and intensity forecasts, was not considered to be necessary for this study of the Irma RI event. Consequently, the upscaling of the FCDI analysis in Domain 2, and the separate 6 h NAVGEM forecast to provide the Domain 1 lateral boundary conditions for the next FCDI analysis have been omitted in this study. This fourth modification of the Elsberry et al. [1] dynamic initialization technique has provided a less complex and more time-efficient approach to demonstrate the impact of high temporal and spatial resolution GOES-16 AMVs on the FCDI analysis and COAMPS-TC 72 h forecasts of the Irma RI event.

One of the challenges in assimilating the strong AMVs near the center of Irma was that the first step in the FCDI is from a cold-start COAMPS-TC that has a bogus vortex in which the model winds may have large (5–6 m s^{-1}) deviations from the AMV observations. Thus, it was important that the nudging term quickly adjusted the model winds toward the AMVs each 15 min segment. The nudging each 15 min of the model winds to the lower density hourly AMVs was also successful, which was in part because the hourly AMVs were smaller as they were generally more than 100 km from the center. The key differences among the 15 min AMV FCDI analysis, the hourly AMV FCDI analysis, and the Control COAMPS-TC initial conditions with a bogus vortex at 18 UTC 3 September, were in the FCDI analyses outflow magnitudes and in how strongly the Irma outflow was connected to adjacent synoptic circulations. The 15 min AMV FCDI had the largest of both factors and the COAMPS-TC initial conditions had the smallest of both factors. It is noted that the second modification of the Elsberry et al. [1] technique to expand the sizes of the Domains 2 and 3 was important in better resolving the Irma outflow connections with the adjacent synoptic circulations.

One of the limitations of this study was that the first set of GOES-16 AMVs was not available until just before the beginning of the Irma RI event, at least according to the NHC working best track (WBT). However, there had been no in situ observations and according to the SATCON the first GOES-16 dataset was at a time when the Irma intensity was decreasing in advance of the RI event. So while the surface wind adjustment was successful in bringing the Irma vortex quite near the target position at the end of the 6 h FCDI analysis, the reliance on a cold start with a bogus vortex based on the NHC WBT rather than the SATCON made validation of the three COAMPS-TC forecasts during the pre-extreme RI period somewhat uncertain. Taking into account the intensity uncertainty at the beginning of the extreme RI period, the three COAMPS-TC forecasts of that first segment of the RI event were generally successful.

The distinguishing feature of this Irma RI event is considered in this study to be the existence and timing of the intermediate constant-intensity (MSLP) period between the extreme RI period and the extended slower RI period. Only the 15 min AMV FCDI-based COAMPS-TC forecast accurately predicted the timing and persistence of constant MSLP that was defined by multiple NOAA and Air Force aircraft observations, and then resumed MSLP deepening of Irma at the correct time and with an accurate rate during the extended slower RI period. Although the Control COAMPS-TC forecast had an earlier and short-lived constant MSLP period, it predicted a rapid decrease in MSLP during the observed 12 h period of constant intensity, and then continued that MSLP deepening through the extended slower RI period. The hourly AMV FCDI-based COAMPS-TC forecast had no indication of that intermediate period of constant intensity as it steadily decreased the MSLP from the beginning of the extreme RI period through the extended slower RI period. Thus, some characteristic of the environment and/or the inner-core Irma vortex and its outflow resolved only by the 15 min AMV FCDI analysis appears to be able to explain all four periods of this Irma RI event.

Comparing the initial conditions and the three z = 12,860 m COAMPS-TC wind forecasts at tau + 24 h and tau + 48 h provides some evidence as to why the 15 min AMV FCDI-based COAMPS-TC forecast was the most successful. First, the 15 min AMV FCDI initial conditions had a stronger outflow toward the northeast that had pushed back to the east a northerly environment flow that was impinging on the outflow in the Control COAMPS-TC and in the hourly AMV FCDI initial conditions. Thus, the 15 min AMV COAMPS-TC tau + 24 h forecast had a stronger outflow in all quadrants that had established direct connections with adjacent synoptic circulations to the northeast as well as to the northwest. By contrast, the Control (hourly AMV) COAMPS-TC had strong outflow but no (only weak to the west) connection to adjacent synoptic circulations, so that all (nearly all) of that strong outflow was subsiding in the near-environment of the Irma vortex at tau + 24 h.

Further analysis is needed to explain how most of those direct connections of the 15 min AMV COAMPS-TC outflow to the adjacent synoptic circulations at tau + 24 h had ended by tau + 48 h, and especially how this change is related to the intermediate constant MSLP period. Strong outflow that extended to larger areas had resumed, but that outflow was being confined by an almost complete

ring of light winds. Nevertheless, this 15 min AMV COAMPS-TC forecast had resumed the rapid deepening at the correct time and that deepening would continue through the extended slower RI period. By contrast, the hourly AMV COAMPS-TC tau + 48 h forecast had a much stronger outflow that extended over a much larger area than at tau + 24 h, and had a more direct connection to the north and had pushed through the region of light winds to the northeast to have direct connection to the northerly environmental flow. The stronger outflow and enhanced direct connections to the adjacent synoptic circulations are consistent with the continuous rapid MSLP deepening in the hourly AMV COAMPS-TC forecast from tau + 24 h through tau + 48 h, but that missed the intermediate constant MSLP period.

Comparison of the initial conditions and the three z = 300 m COAMPS-TC wind forecasts at tau + 24 h forecasts reveals only subtle differences. Both of the 15 min AMV and the hourly AMV FCDI analyses have highly asymmetric vortex wind structures compared to the symmetric bogus vortex in the Control COAMPS-TC at the initial time of 18 UTC September. By tau + 24 h the hourly AMV COAMPS-TC has intensified with the strongest 300 m winds in the western semicircle versus in the northern semicircle for the 15 min AMV COAMPS-TC semicircle. By tau + 48 h the hourly AMV COAMPS-TC 300 m wind field is again highly asymmetric and even though it has a stronger wind than the 15 min AMV COAMPS-TC forecast, it is not evident how these differences are related to the intermediate constant MSLP period that was (was not) predicted by the 15 min (hourly) AMV COAMPS-TC forecast. A future study will examine the horizontal and vertical structure of the predicted Irma vortex to determine whether these structure changes are related to the intermediate constant MSLP period.

Finally, the Lewis et al. [6] Control and high-density GOES-16 AMV HWRF initializations at 18 UTC 3 September and the subsequent 72 h HWRF model forecasts of the Irma RI event have been compared with the Control COAMPS-TC initial conditions and the 15 min GOES-16 AMV FCDI analysis and the subsequent 72 h COAMPS forecasts. Due to the sophisticated HWRF vortex initialization procedure, the Lewis et al. [6] tau = 0 h MSLP for both the Control and the high-density AMV HWRF intensity forecasts were equal to the NHC best-track value at the initial time of 18 UTC 3 September. However, both HWRF model forecasts rapidly deepened the MSLP by 15 mb in 12 h and more than 25 mb in 24 h. As was the case for the Control COAMPS-TC MSLP forecast, the Control HWRF forecast had an earlier 12 h period of constant MSLPs before the intermediate constant MSLP period in the NHC best track that is based on aircraft observations. Indeed, the Control HWRF forecast had an 8 mb deepening during that 12 h constant MSLP period, and continued to rapidly deepen Irma until tau + 72 h with a MSLP of 908 mb, which is an overdeepening by 10 mb. It was somewhat surprising that the HWRF forecast from an initialization that included the high-density AMVs continued that rapid deepening right through that constant MSLP period.

One key to the rapid deepening in the Control HWRF forecast may have been the HWRF outflow toward the north was so strong that the outflow had pushed back the impinging northerly environmental flow encroaching on the outflow as in the Control COAMPS-TC initial conditions. However, the continuous band of light winds between the outflow and the northerly environmental flow to the northeast in the Control HWRF initial conditions also means that the outflow has no pathway to connecting with the northerly environmental flow to the east, which was a contributor to the rapid deepening in the 15 min AMV and hourly AMV FCDI-based COAMPS-TC forecasts. In tau + 24 h, tau + 48 h, and tau + 72 h Control HWRF forecasts (Figure 18b, Figure 18c, and Figure 18d, respectively), the band of light winds almost completely encircles the Irma outflow so that the direct connection with adjacent synoptic circulations becomes more and more inhibited. The exception is the southward outflow at tau + 24 h and tau + 48 h that appears to contribute to the easterly jet maximum near 9° N, 65° W in Figure 18c. In summary, the rapid deepening in the Control HWRF evidently occurs via a different mode than in the FCDI-based COAMPS-TC forecasts in which outflow bursts lead to the establishment of direct connections with the adjacent synoptic flows. In this Control HWRF forecast the outflow appears to be confined or constrained to a smaller area around the center position.

The HWRF initialization of the z = 12,860 m wind field with the high-density AMV dataset (Figure 19a) is quite similar to the Control HWRF initialization in the near-environment of Irma. Rather than the GOES AMVs contributing to a stronger outflow as in the 15 min AMV FCDI-based initial conditions (Figure 11a), the magnitude and the areal extent of the HWRF outflow are smaller. Except for the outflow toward the southwest at tau + 24 h in the HWRF forecast (Figure 19b), the outflow magnitude and areal extent are smaller than in the Control HWRF forecast (Figure 18b). The same confinement or constraint of the outflow leading to the absence of direct connections with the adjacent synoptic circulations applies at tau + 24 h and at tau + 48 h as in the Control HWRF forecast. Consequently, the outflow magnitudes and areal extents remain small at these times in the high-density AMV HWRF forecast. It is only at tau +72 h (Figure 19d) that a northward outflow branch establishes a weak direct connection with the northerly environmental flow to the east, which was a major feature in the 15 min AMV FCDI-based COAMPS-TC forecast at tau + 72 h (Figure 11d). Thus, the rapid deepening in the high-density AMV HWRF forecast evidently occurs via a different mode than in the FCDI-based COAMPS-TC forecasts in which outflow bursts lead to the establishment of direct connections with the adjacent synoptic flows.

4.2. Concluding Remarks

This study is a part of an Office of Naval Research project to understand, analyze, and predict RI in tropical cyclones, and the central focus is on the heightened observational opportunities from the new-generation geostationary meteorological satellites such as GOES-16 to make advances in all of those RI facets. While the earlier Elsberry et al. [1] study utilized special reprocessed GOES-13 AMVs that attempted to simulate what was to become available from the new-generation targeted meso scans, this is one of the first studies (Lewis et al. [6] is another) to utilize AMVs from the 1 min images within the meso scan domain to achieve extremely high spatial resolution over the outflow dome. Consequently, it was possible to monitor the evolution of that outflow dome every 15 min during the six-hour data assimilation cycle in Hurricane Irma. These continuous (15 min) FCDI analyses also have the capability to specify the environmental wind fields that were interacting with the outflow. The demonstration here was the benefit in creating the initial conditions for a 72 h COAMPS-TC forecast of the Irma RI. The next step is to generate FCDI analyses every 15 min prior to, during, and following that RI event for diagnostic studies, model initial conditions, and model validation studies. A specific objective is to collaborate with the NOAA Hurricane Research Division group that has generated analyses based on the aircraft missions in Hurricane Irma [14], as such in situ observations are critical for evaluating the fidelity of the FCDI analyses. In addition, aircraft missions can provide the horizontal and vertical structure of the Irma vortex, which will be very helpful in validating the FCDI analyses at z = 300 m in Figure 14, and testing various hypotheses regarding mesoscale vortices within the eyewall.

The primary objective of the comparisons with the Lewis et al. [6] study that utilized the HWRF initialization and the HWRF model forecast of the Irma RI was not to draw any conclusions about the capability of the HWRF model versus the COAMPS-TC model in predicting RI. Rather, the purpose was to demonstrate that the FCDI approach is an alternative to how the HWRF assimilates the high spatial and temporal resolution AMVs. While this is just one example (indeed, one of the major take-aways of this study is that many such GOES-16 AMV datasets are urgently needed), it is asserted that the FCDI is an additional approach to take advantage of the opportunity from the GOES-16 to advance understanding, analyses, and predictions of RI events in tropical cyclones.

Supplementary Materials: The following are available online at http://www.mdpi.com/2073-4433/11/11/1200/s1, Figure S1: As in Figure 6, except here with the CIMSS hourly GOES-13 AMVs rather than the GOES-16 AMVs illustrating the Domain 3 FCDI analyses of the z = 12,860 m wind vectors (m s^{-1}; color bar at bottom and 20 m s^{-1} length indicated by arrow in middle) starting from cold-start COAMPS-TC wind vectors in panel (a) and then hourly AMV-based FCDI analyses at (b) tau = 2 h, (c) tau = 4 h, and (d) tau = 6 h, Figure S2: As in Figure 7, except here for the hourly GOES-13AMV-based FCDI z = 12,860 m wind increments (m s^{-1}; color bar at bottom and 2 m s^{-1} vector length indicated by arrow in middle) at (a) tau = 0 h, (b) tau = 15 min, (c) 30 min, and (d) 45 min,

Figure S3: As in Figure 9 for inner-region Domain 3 z = 300 m isotachs at 3 m s^{-1} interval, from 3 m s^{-1} to 54 m s^{-1} for (a) cold-start COAMPS-TC initial conditions at 12 UTC 3 September, and at 18 UTC 3 September (b) 15-min AMV FCDI analysis (c) six hour COAMPS-TC forecast, and (d) hourly AMV FCDI analysis, Figure S4: CIMSS Control HWRF (a) Initialization for the z = 250 m wind vectors (m $s^{-1,}$ color bar at bottom) at 18 UTC 3 September, and then the HWRF model forecasts at (b) tau + 24 h, (c) tau + 48 h, and (d) tau + 72 h (provided by William E. Lewis, CIMSS), Figure S5: As in Figure S4, except with (a) the CIMSS high-density AMV dataset included in the HWRF vortex initialization, and then the HWRF forecasts at (b) tau + 24 h, (c) tau + 48 h, and (d) tau + 72 h (provided by William E. Lewis, CIMSS).

Author Contributions: Conceptualization, R.L.E. and C.S.V. have collaborated over a number of years on the opportunities and challenges with the new-generation meteorological satellites such as GOES-16. Methodology, J.W.F. has conceived the methodology for displaying the GOES-16 AMVs, and R.L.E., M.P., and H.-J.C. have jointly developed the methodology for assimilating the high-density AMVs via the FCDI dynamic initialization technique. Software coding has been done by H.-J.C. Validation has been done by R.L.E. and H.-J.C. with the assistance of M.P. and J.W.F. Administrative overview has been by R.L.E., M.P., and Q.W. Writing, R.L.E. has been responsible for the text and H.-J.C. and J.W.F. have been responsible for the figures. All authors have read and agreed to the published version of the manuscript.

Funding: R.L.E. and M.P. have been funded by Office of Naval Research (ONR) Grants N000141712160 and N0001912465, and R.L.E. has also been funded by ONR Grant N000142012180. J.W.F. and H.-J.C. have been funded by ONR Grant N0001420WX01445. C.S.V. has been supported by ONR Grant N000141613033. Q.W. and H.-J.C. have been funded by ONR Grant N0001419WX01558.

Acknowledgments: We thank Penny Jones for her excellent support of the manuscript preparation.

Conflicts of Interest: The authors declare no conflict of interest.

Appendix A

In Elsberry et al. [1], the COAMPS-TC track forecasts of Hurricane Joaquin (2015) with the NAVGEM (their Figure 9a) and with the NCEP GFS (their Figure 10a) background fields both had early track deviations from the recent-past motion vector that may be attributed to position uncertainty during the assimilation period. Most importantly, when the new FCDI described in Section 2.1.1 was tested during the early stage of Joaquin with a cold-start COAMPS-TC, the predicted motion was a slow drift to the west rather than to the southwest toward the Bahamas, and intense deep convection associated with a "grid point vortex" to the south of the actual center led to highly erratic motion vectors. Therefore, the third modification in developing the FCDI technique was to constrain the near-surface wind distribution to follow a prescribed target path during each 6 h assimilation period that originates at the initial TC position and terminates at a projected location based on the 6 h warning center fix or the averaged 30 min SATCON datasets if available.

The first objective is to constrain the boundary layer and its associated convective process physics to continue to have realistic characteristics relative to the vortex center while being nudged toward the target path based on either the new storm fix position or the SATCON position. The second objective of the continued adjustment of the surface wind field to move along the target pathway is that the FCDI analyzed 6 h position is then sufficiently close to the next warning position that the next assimilation cycle may then begin from that previous assimilation 6 h position. Therefore, no vortex relocation or introduction of a bogus vortex at the warning position is required. An example of a target pathway and surface wind adjustments is given in Figure 10a.

Assuming a new AMV dataset will be available each 15 min, the 6 h target path is broken into 24 iteration segments at which times the near-surface wind components in a 1500 m deep layer within a 300 km by 300 km domain is used to define a nudging wind increment field. For example, the zonal wind increments are defined as ($U_{target} - U_{model}$) where U_{target} represents the TC vortex zonal wind components after 15 min if the vortex center had been displaced by a grid point (Domain 3 grid interval) along the target path. During the next 15 min, the zonal wind Equation (A1) within the near-surface wind domain shown in Figure A1 will have a nudging term

$$\frac{\partial U}{\partial t} = [\text{other terms}] - \propto \left[U_{target} - U_{model}\right] \quad \text{(A1)}$$

which will tend to adjust the vortex toward one grid point to the north and one grid point to the east. An example of the vector wind increments at 1050 m elevation for a target 60 m s^{-1} vortex with a radius of maximum wind (RMW) of 25 km that has been moved one grid point (5 km) to the north and one grid point to the east is given in Figure A1.

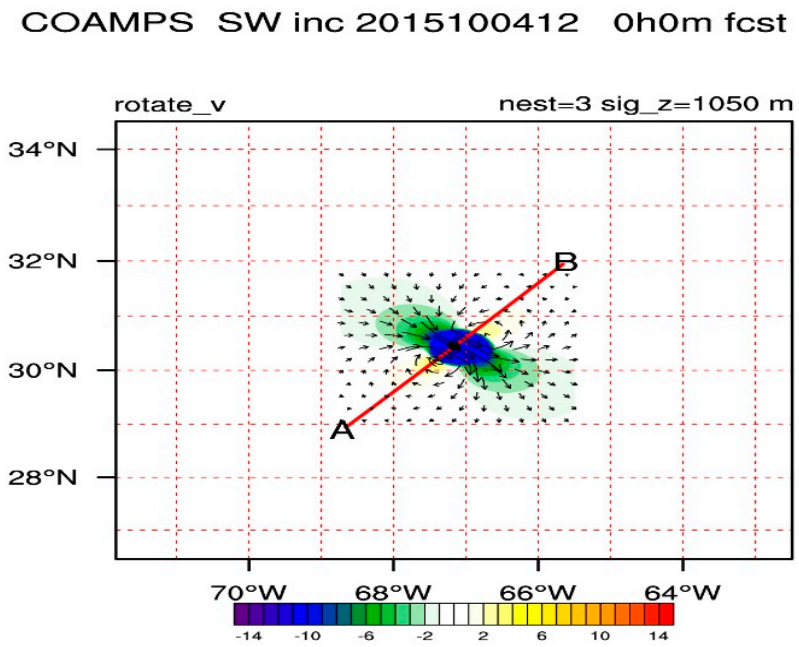

Figure A1. Wind increment vectors (m s^{-1}, color scale along bottom) for nudging a 60 m s^{-1} vortex with a RMW = 25 km to the north and to the east by one grid point. The red line representing the target path connects the starting position A with the ending position B.

References

1. Elsberry, R.L.; Hendricks, E.A.; Velden, C.S.; Bell, M.M.; Peng, M.; Casas, E.; Zhao, Q. Demonstration with special TCI-15 datasets of potential impacts of new-generation satellite atmospheric motion vectors on Navy regional and global models. *Weather Forecast.* **2018**, *33*, 1617–1637. [CrossRef]
2. Hendricks, E.A.; Elsberry, R.L.; Velden, C.S.; Jorgensen, A.C.; Jordan, M.S.; Creasey, R.L. Environmental factors and internal processes contributing to the interrupted rapid decay of Hurricane Joaquin (2015). *Weather Forecast.* **2018**, *33*, 1251–1262. [CrossRef]
3. Elsberry, R.L.; Buholzer, N.; Velden, C.S.; Jordan, M.S. Satellite-based observations of nonlinear relationships between vertical wind shear and intensity changes during the lifecycle of Hurricane Joaquin (2015). *Weather Forecast.* **2020**, *35*, 939–958. [CrossRef]
4. Berg, R.L. Hurricane Joaquin (28 September–7 October 2015). In *National Hurricane Center Tropical Cyclone Report AL112015*; NOAA/National Hurricane Center: Miami, FL, USA, 2016; 36p. Available online: www.nhc.noaa.gov/data/tcr/AL112015_Joaquin.pdf (accessed on 10 March 2019).
5. Cangialosi, J.P.; Latto, A.S.; Berg, R. *National Hurricane Center Tropical Cyclone Report, Hurricane Irma AL112017*; NOAA/National Hurricane Center: Miami, FL, USA, 2018; 111p. Available online: www.nhc.noaa.gov/data/tcr/AL112017_Irma.pdf (accessed on 10 March 2019).
6. Lewis, W.E.; Velden, C.S.; Stettner, D. Strategies for assimilating high-density atmospheric motion vectors into a regional tropical cyclone forecast model (HWRF). *Atmosphere* **2020**, *11*, 673. [CrossRef]
7. Stettner, D.; Velden, C.S.; Rabin, R.; Wanzong, S.; Daniels, J.; Breskey, W. Development of enhanced vortex-scale atmospheric motion vectors for hurricane applications. *Remote Sens.* **2019**, *11*, 1981. [CrossRef]
8. Bell, M.M.; Montgomery, M.T.; Emanuel, K.E. Air-sea enthalpy and momentum exchange at major hurricane speeds observed during CBLAST. *J. Atmos. Sci.* **2012**, *65*, 3197–3222. [CrossRef]
9. Dudhia, J. Four-dimensional variational data assimilation for WRF formulation and preliminary results. *Mon. Weather Rev.* **2009**, *137*, 299–314.

10. Shewchuk, J.D.; Elsberry, R.L. Improvement of a baroclinic typhoon motion prediction system by adjustment of the initial wind field. *Mon. Weather Rev.* **1978**, *106*, 713–718. [CrossRef]
11. Minamida, M.; Zhang, F. Assimilation of all-sky radiances from Himawari-8 and impacts of moisture and hydrometer initialization on convection-permitting tropical cyclone prediction. *Mon. Weather Rev.* **2018**, *146*, 3241–3258. [CrossRef]
12. Sawada, M.; Ma, Z.; Mehra, A.; Tallapragada, V.; Oyama, R.; Shimoji, K. Assimilation of Himawari-8 rapid-scan atmospheric motion vectors on tropical cyclone in HWRF system. *Atmosphere* **2020**, *11*, 601. [CrossRef]
13. Velden, C.S.; Herndon, D. A consensus approach for estimating tropical cyclone intensity from meteorological satellites: SATCON. *Weather Forecast.* **2020**, *35*, 1642–1662. [CrossRef]
14. Fischer, M.S.; Rogers, R.F.; Reasor, P.D. The rapid intensification and eyewall replacement cycles of Hurricane Irma (2017). *Mon. Weather Rev.* **2020**, *148*, 961–1004. [CrossRef]
15. DeMaria, M.; Kaplan, J. A statistical hurricane prediction scheme (SHIPS) for the Atlantic basin. *Weather Forecast.* **1994**, *8*, 209–220. [CrossRef]
16. Feng, J.; Wang, X. Impact of assimilating upper-level dropsonde observations collected during the TCI field campaign on the prediction of intensity and structure of Hurricane Patricia (2015). *Mon. Weather Rev.* **2019**, *147*, 3069–3089. [CrossRef]